Coordination of Leaf Photosynthesis, Transpiration, and Structural Traits in Rice and Wild Relatives (Genus *Oryza*)[1][W][OA]

Rita Giuliani, Nuria Koteyeva, Elena Voznesenskaya, Marc A. Evans, Asaph B. Cousins, and Gerald E. Edwards*

School of Biological Sciences, Washington State University, Pullman, Washington 99164–4236 (R.G., A.B.C., G.E.E.); Laboratory of Anatomy and Morphology, V.L. Komarov Botanical Institute of the Russian Academy of Sciences, 197376 St. Petersburg, Russia (N.K., E.V.); and Department of Mathematics, Washington State University, Pullman, Washington 99164–3113 (M.A.E.)

ORCID ID: 0000-0002-6640-1654 (G.E.E.).

The genus *Oryza*, which includes rice (*Oryza sativa* and *Oryza glaberrima*) and wild relatives, is a useful genus to study leaf properties in order to identify structural features that control CO_2 access to chloroplasts, photosynthesis, water use efficiency, and drought tolerance. Traits, 26 structural and 17 functional, associated with photosynthesis and transpiration were quantified on 24 accessions (representatives of 17 species and eight genomes). Hypotheses of associations within, and between, structure, photosynthesis, and transpiration were tested. Two main clusters of positively interrelated leaf traits were identified: in the first cluster were structural features, leaf thickness ($Thick_{leaf}$), mesophyll (M) cell surface area exposed to intercellular air space per unit of leaf surface area (S_{mes}), and M cell size; a second group included functional traits, net photosynthetic rate, transpiration rate, M conductance to CO_2 diffusion (g_m), stomatal conductance to gas diffusion (g_s), and the g_m/g_s ratio. While net photosynthetic rate was positively correlated with g_m, neither was significantly linked with any individual structural traits. The results suggest that changes in g_m depend on covariations of multiple leaf (S_{mes}) and M cell (including cell wall thickness) structural traits. There was an inverse relationship between $Thick_{leaf}$ and transpiration rate and a significant positive association between $Thick_{leaf}$ and leaf transpiration efficiency. Interestingly, high g_m together with high g_m/g_s and a low S_{mes}/g_m ratio (M resistance to CO_2 diffusion per unit of cell surface area exposed to intercellular air space) appear to be ideal for supporting leaf photosynthesis while preserving water; in addition, thick M cell walls may be beneficial for plant drought tolerance.

Leaves have evolved in different environments into a multitude of sizes and shapes, showing great variation in morphology and anatomy (Evans et al., 2004). However, all leaf typologies share common functions associated with chloroplasts, namely to intercept sunlight, take up CO_2 and inorganic nitrogen, and perform photosynthesis as a primary process for growth and reproduction.

Investigating relationships between leaf anatomy and photosynthetic features (CO_2 fixation, which involves physical and biochemical processes and loss of water by transpiration) could lead to the identification of structural features for enhancing crop productivity and improve our understanding of plant evolution and adaptation (Evans et al., 2004).

Stomata, through which CO_2 and water vapor diffuse into and out of the leaf, are involved in the regulation and control of photosynthetic and transpiration responses (Jarvis and Morison, 1981; Farquhar and Sharkey, 1982). Besides stomata distribution patterns between the abaxial and adaxial lamina surfaces (Foster and Smith, 1986), stomatal density and size are leaf anatomical traits contributing to build the leaf stomatal conductance to gas diffusion (g_s). This is calculated as the reciprocal of the stomatal resistances to gas diffusion; stomatal control results in a lower concentration of CO_2 in the leaf mesophyll (M) intercellular air space (C_i) than in the atmosphere (C_a; Nobel, 2009).

Leaf M architecture greatly contributes to the pattern of light attenuation profiles within the lamina (Terashima and Saeki, 1983; Woolley, 1983; Vogelmann et al., 1989; Evans, 1999; Terashima et al., 2011) and affects CO_2 diffusion from the intercellular air space (IAS) to the chloroplast stroma. Therefore, it influences photosynthetic activity (Flexas et al., 2007, 2008) and can have effects on leaf hydrology and transpiration (Sack et al., 2003; Brodribb et al., 2010; Ocheltree et al., 2012). In addition, M architecture sets boundaries for leaf photosynthetic responses to changing environmental conditions (Nobel et al., 1975).

Fortunately, several methodologies are currently available (Flexas et al., 2008; Pons et al., 2009) to determine M conductance to CO_2 diffusion (g_m), expressed per unit of

[1] This work was supported by the International Rice Research Institute (C_4 rice program) through a grant by the Bill and Melinda Gates Foundation, by the U.K. Department for International Development, and by the National Science Foundation (Major Research Instrumentation grant no. 0923562 and grant no. MCB 1146928).

* Corresponding author; e-mail edwardsg@wsu.edu.

The author responsible for distribution of materials integral to the findings presented in this article in accordance with the policy described in the Instructions for Authors (www.plantphysiol.org) is: Gerald E. Edwards (edwardsg@wsu.edu).

[W] The online version of this article contains Web-only data.

[OA] Open Access articles can be viewed online without a subscription.

www.plantphysiol.org/cgi/doi/10.1104/pp.113.217497

leaf surface area. It is calculated as the reciprocal of the cumulated partial resistances exerted by leaf structural traits and biochemical processes from the substomatal cavities to photosynthetic sites (Evans et al., 2009; Nobel, 2009). The resistance to CO_2 diffusion in the liquid phase is 4 orders of magnitude higher than in the gaseous phase (Nobel, 2009); therefore, the changes in CO_2 concentration in the leaf gas phase are small in comparison with the changes in the liquid phase (Niinemets, 1999; Aalto and Juurola, 2002; Nobel, 2009). In the liquid phase, the resistance to CO_2 transfer is built from contributions by the cell walls, the plasmalemma, cytoplasm, chloroplast membranes, and stroma (Tholen and Zhu, 2011; Tholen et al., 2012); in addition, it involves factors associated with the carboxylation reaction (Kiirats et al., 2002; Evans et al., 2009). Thus, the concentration of CO_2 in the chloroplasts (C_c) is lower than C_i and can limit photosynthesis.

At steady state, the relationships between the leaf net photosynthetic rate (A), the concentrations of CO_2, and the stomatal conductance to CO_2 diffusion (g_{s_CO2}) and g_m are modeled based on Fick's first law of diffusion (Nobel, 2009) as:

$$A = g_{s\_CO2}(C_a - C_i) = g_m(C_i - C_c) \quad (1)$$

where C_a, C_i, and C_c are as defined above (Flexas et al., 2008).

The magnitude of g_m has been found to correlate with certain leaf structural traits in some species, in particular with the M cell surface area exposed to IAS per (one side) unit of leaf surface area (S_{mes}) and its extent covered by chloroplasts (S_{chl}; Evans and Loreto, 2000; Slaton and Smith, 2002; Tholen et al., 2012). From a physical modeling perspective, increasing S_{mes} provides more pathways acting in parallel for CO_2 diffusion (to and from the chloroplasts) per unit of leaf surface area; thus, it tends to reduce the resistance to CO_2 movement into the M cells and to increase g_m (Evans et al., 2009; Nobel, 2009). A number of leaf structural traits affect S_{mes}, including leaf thickness, cell density, cell volume and shape, and the fraction of the M cell walls in contact with the IAS (Terashima et al., 2001, 2011), and the degree they are linked to S_{mes} can vary between species (Slaton and Smith, 2002; Terashima et al., 2006). In particular, the presence of lobes on M cells, which are prominent in some *Oryza* species, may contribute to g_m through increasing S_{mes} (Sage and Sage, 2009; Terashima et al., 2011; Tosens et al., 2012). The M cell wall can provide resistance in series for M CO_2 diffusion (Nobel, 2009); thicker cell walls may increase resistance to CO_2 movement into the M cells and decrease g_m (Terashima et al., 2006, 2011; Evans et al., 2009).

Other leaf traits, such as M porosity (the fraction of M volume occupied by air spaces [Vol_{IAS}]), has been shown to have a positive correlation with g_m in some species (Peña-Rojas et al., 2005), but the association may be mediated by light availability (Slaton and Smith, 2002). Leaf thickness ($Thick_{leaf}$) tends to be negatively linked to g_m, and it may set an upper limit for the maximum g_m, according to Terashima et al. (2006), Flexas et al. (2008), and Niinemets et al. (2009).

With respect to leaf structural traits and water relations, $Thick_{leaf}$ may increase the apoplast path length (resistances in series; Nobel, 2009) in the extra-xylem M (Sack and Holbrook, 2006; Brodribb et al., 2007) for water to reach the evaporation sites, which could decrease the conductance of water through the M and lower the transpiration rate. Interestingly, while thicker M cell walls may reduce g_m, they can enable the development of higher water potential gradients between the soil and leaves, which can be decisive for plant survival and longevity under drought conditions (Steppe et al., 2011).

The purpose of this study was to provide insight into how the diversity of leaf structure relates to photosynthesis and transpiration among representative cultivated species and wild relatives in the genus *Oryza*. This includes, in particular, identifying leaf structural features associated with the diffusion of CO_2 from the atmosphere to the chloroplasts, photosynthesis, transpiration efficiency (A/E), and drought tolerance. The genus consists of 10 genomic groups and is composed of approximately 24 species (the number depending on taxonomic preferences; Kellogg, 2009; Brar and Singh, 2011), including the cultivated species *Oryza sativa* and *Oryza glaberrima*. *Oryza* species are distributed around the world, and they exhibit a wide range of phenotypes, with annual versus perennial life cycles and sun- versus shade-adapted species (Vaughan, 1994; Vaughan et al., 2008; Brar and Singh, 2011; Jagadish et al., 2011). This diversity in the genus is an important resource, which is being studied to improve rice yield, especially under unfavorable environmental conditions. In particular, *O. glaberrima*, *Oryza australiensis*, and *Oryza meridionalis* are of interest as drought-tolerant species (Henry et al., 2010; Ndjiondjop et al., 2010; Scafaro et al., 2011, 2012), while *Oryza coarctata* is salt tolerant (Sengupta and Majumder, 2010). In this study, a total of 43 leaf functional and structural parameters were collected on 24 accessions corresponding to 17 species within eight genomes (Table I) to represent the spectrum of the leaf diversity in the genus *Oryza*.

For evaluating aspects of photosynthesis, the model in Equation 1 was considered, and all the listed functional variables, A, g_{s_CO2}, $(C_a - C_i)$, g_m, and $(C_i - C_c)$, were determined. In addition, among the leaf functional traits, the M resistance to CO_2 diffusion per unit of cell surface area exposed to IAS (reciprocal of g_m/S_{mes}) was calculated as described by Evans et al. (2009): it represents the resistance to CO_2 diffusion from IAS to chloroplasts in a liquid solution through cell wall and membranes (Nobel, 2009). Leaf transpiration rate (E), A/E, the intrinsic A/E (ratio between A and stomatal conductance to water vapor diffusion [g_{s_H2O}]), g_m/g_{s_CO2} (representing the coordination between g_m and g_s), and the carbon isotope composition of leaf biomass ($\delta^{13}C$; calculated as $^{13}C/^{12}C$) were determined. The value of $\delta^{13}C$ has been recognized as a potential indicator of leaf A/E: increased limitations on photosynthesis by decreased g_s can lead to higher A/g_{s_H2O} ratios and less discrimination against assimilation of $^{13}CO_2$ (for

Table I. *Oryza accessions used in this study and identified by the assigned numbers*

Leaf functional measurements were performed on all accessions; structural measurements were made on accessions labeled with asterisks (for *O. sativa* cv IR72 and *O. australiensis* 22, structural measurements were only made on stomata but not other traits). Genomes for *Oryza* species are according to Brar and Singh (2011). Life cycle is as follows: A = annual; B = biennial; *P* = poliennial. Habitat is as follows: S = shade; S-Sh = sun-shade.

Genome	Species	Life Cycle	Habitat	Accession	No.
AA	*O. barthii*	A	S	PI 590400*	1
AA	*O. glaberrima*	A	S	PI 450430*	2
AA	*O. glumaepatula*	P	S	PI 527362*	3
AA	*O. longistaminata*	P	S	IRGC 101207*	4
AA	*O. longistaminata*	P	S	IRGC 101754	5
AA	*O. meridionalis*	A/P	S	IRGC 93265*	6
AA	*O. nivara*	A/B	S	PI 590405*	7
AA	*O. rufipogon*	P	S	PI 104640	8
AA	*O. rufipogon*		S	PI 590421*	9
AA	*O. sativa*	A	S	IR64*	10
AA	*O. sativa*	A	S	IR72	11
BB	*O. punctata*	A	S-Sh	IRGC 105690*	12
BBCC	*O. minuta*	P	S-Sh	IRGC 101141*	13
CC	*O. officinalis*	P	S-Sh	PI 59412*	14
CC	*O. rhizomatis*	P	S	IRGC 101609	15
CC	*O. rhizomatis*	P	S	IRGC 105950*	16
CCDD	*O. alta*	P	S-Sh	PI 590398*	17
CCDD	*O. latifolia*	P	S-Sh	IRGC 100959*	18
CCDD	*O. latifolia*	P	S-Sh	IRGC 105173	19
EE	*O. australiensis*	P	S	IRGC 101397*	20
EE	*O. australiensis*	P	S	IRGC 105277*	21
EE	*O. australiensis*	P	S	IRGC 86527	22
FF	*O. brachyantha*	B	S	IRGC 101232*	23
HHKK	*O. coarctata*	P	S	IRGC 104502*	24

review, see Farquhar et al., 1989); the leaf A/E may also be positively linked to the g_m/g_s ratio (Flexas et al., 2008, 2013; Barbour et al., 2010). With respect to leaf structure, the stomatal density, stomatal pore length, and indices of stomatal pore area on both lamina sides (according to Sack et al., 2003), the $Thick_{leaf}$, Vol_{IAS}, S_{mes}, S_{chl}, area of M cell section (a_{cell}) in leaf cross sections, cell wall thickness ($Thick_{cw}$), and M cell surface lobing (Lob_{cell}) were the principal traits estimated. A statistical multivariate analysis (Child, 2006) was employed to identify clusters of highly interrelated leaf traits; trait-to-trait correlation analysis was carried out to further examine leaf structural, functional, and structural-functional relationships.

The following are the main hypotheses examined in this study. (1) Leaf thickness will be associated with certain M structural features. (2) g_m will be coordinated with M structural traits. (3) A will be correlated with g_s, g_m, and E. (4) Leaf structural traits will be involved in the relationship between A and E, which will affect leaf A/E. (5) The g_m/g_s ratio will be positively correlated with leaf A/E; associations with high $Thick_{cw}$ could have implications for plant drought tolerance.

RESULTS

Significance of ANOVA for Structural and Functional Leaf Traits

The accessions analyzed in this study, and the corresponding species and genomes, are listed in Table I; and, the list of leaf traits determined are shown in Table II. The overall significance for differences among *Oryza* genomes, species nested within genomes, and accessions nested within species and genomes, for each leaf structural and functional trait, are reported in Table III. Among genomes, there were significant differences in most structural and functional traits. Among species nested within genomes, there were significant differences in about half of the leaf traits, including stomatal pore area index in the abaxial lamina surface ($I_{st}ab$), mean $Thick_{leaf}$, total S_{mes}, $Thick_{cw}$, maximum carboxylation efficiency (CE), g_m, and A. Among accessions nested within species and genomes, there were significant differences in only a few leaf traits, notably $I_{st}ab$, $Thick_{cw}$, g_m, A, E, and A/E.

For each leaf trait, mean values ($\pm$SE) per *Oryza* genome, species, and accession are reported in Supplemental Tables S1, S2, and S3, respectively. In addition, for each trait, corresponding letters of statistical significance ($P < 0.05$) between genomes, between *Oryza* species nested within genomes, and between *Oryza* accessions nested within species and genomes are reported in Supplemental Tables S1, S2, and S3, respectively.

Differences in Leaf and Cell Structural Traits across Accessions

Light and electron micrographs of leaf cross sections for five representative species of *Oryza* are shown in Figure 1. These images illustrate variation in leaf

thickness and shape, the structure of M cells including lobe development, the positions of organelles, and cell area occupied by the vacuole. The adaxial surface of leaves ranges from being relatively flat (Fig. 1, A, D, and J) to having deep invaginations with protrusions above the veins (by extension of bundle sheath and adjacent M cells), as observed, in particular, in *Oryza brachyantha* (Fig. 1G) and *O. coarctata* (Fig. 1M). In all species studied, the mitochondria and peroxisomes are preferentially located internal to the chloroplasts, with the latter being appressed to the plasma membrane (Fig. 1, F, I, L, and O).

The minimum and maximum means within *Oryza* accessions for each leaf trait quantified by microscopy, are shown in Table III (see mean trait values for each accession in Supplemental Table S3). There is an approximately 2-fold difference in $Thick_{leaf}$ across accessions (from approximately 58 to 125 μm). *Oryza rufipogon* 9 (Fig. 1D) and *O. brachyantha* (Fig. 1G) have the thinnest leaves; *O. australiensis* 21 (Fig. 1J), *O. australiensis* 20, *Oryza rhizomatis* 16, and *O. coarctata* (Fig. 1M) have the thickest leaves. The Vol_{IAS} is lowest in *O. brachyantha* and highest (approximately 1.8 times) in *O. australiensis* 20.

Across accessions, 89% (overall mean) of S_{mes} is covered by chloroplasts; the lowest values were 63% for *O. glaberrima* and 67% for *O. meridionalis*; all other values are above 83% (calculations are based on S_{mes} and S_{chl} data in Supplemental Table S3). There is an approximately 3-fold difference across accessions in S_{mes} (and S_{chl}); *Oryza glumaepatula* 3 had the lowest (8.8 $\mu m^2\ \mu m^{-2}$) and *O. coarctata* had the highest (24.4 $\mu m^2\ \mu m^{-2}$) S_{mes} values. The a_{cell} varied approximately 4-fold across accessions (lowest in *O. brachyantha* to highest in *Oryza latifolia* 18). There is a 1.5-fold difference in the extent of Lob_{cell}, which was lowest in *O. brachyantha* (1.06 $\mu m\ \mu m^{-1}$), high in *O. rufipogon* 9 and *O. sativa* cv IR64, and highest in *Oryza barthii* (1.45 $\mu m\ \mu m^{-1}$). $Thick_{cw}$ varied approximately 1.5-fold (from 0.125 μm in *O. rufipogon* 9, to 0.190 μm in *Oryza minuta*).

The fraction of M cell wall covered by chloroplasts (CW_{chl}) was lowest in *O. glaberrima* (approximately 74%) and highest in *Oryza nivara* 7 (approximately 94%); most accessions have CW_{chl} greater than 85% (Supplemental Table S3). Among accessions, the fraction of M cell wall exposed to the IAS (CW_{IAS}) ranged

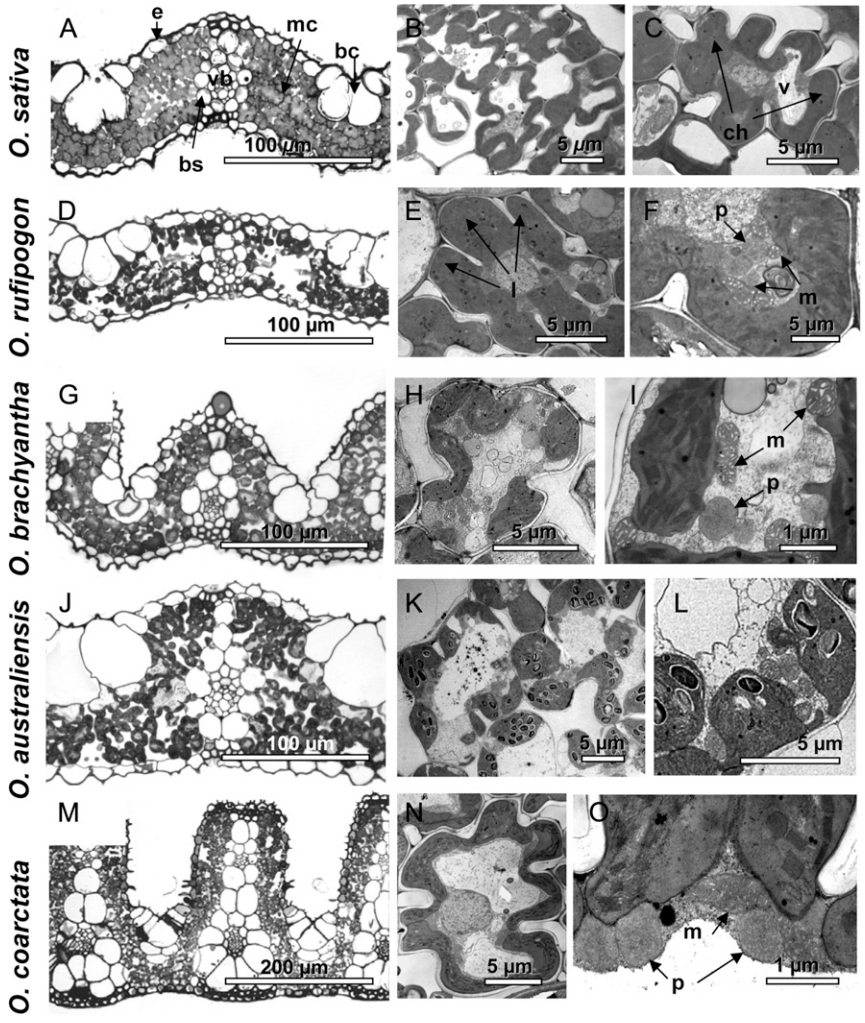

Figure 1. Light (left panels) and electron (middle and right panels) microscopy images of leaf anatomy in representative *Oryza* species (A–C, *O. sativa* cv IR64; D–F, *O. rufipogon* 9; G–I, *O. brachyantha*; J–L, *O. australiensis* 21; M–O, *O. coarctata*). A, D, G, J, and M, Leaf cross-sections. B, C, E, H, K, and N, M cell shape, vacuole development, distribution of chloroplasts, and development of lobes. F, I, L, and O, Positions of mitochondria and peroxisomes internal to the chloroplasts. bc, Bulliform cells; bs, bundle sheath; ch, chloroplast; e, epiderm; l, lobes; m, mitochondria; mc, mesophyll cell; n, nucleus; p, peroxisomes; v, vacuole; vb, vascular bundle.

Table II. *List of leaf traits estimated in this study, and symbols and units adopted*

Trait Category/Trait	Symbol	Unit
Leaf structural traits		
Stomatal density in the abaxial lamina surface	D_{st} ab	mm^{-2}
Stomatal density in the adaxial lamina surface	D_{st} ad	mm^{-2}
Stomatal pore length in the abaxial lamina surface	L_{st} ab	μm
Stomatal pore length in the adaxial lamina surface	L_{st} ad	μm
Stomatal pore area index in the abaxial lamina surface	I_{st} ab	$mm^2\ mm^{-2}$
Stomatal pore area index in the adaxial lamina surface	I_{st} ad	$mm^2\ mm^{-2}$
Stomatal pore area index per unit (one side) of lamina surface area	I_{st}	$mm^2\ mm^{-2}$
Leaf thickness	$Thick_{leaf}$	μm
Fraction of leaf mesophyll volume occupied by intercellular air space	Vol_{IAS}	%
Total mesophyll cell surface area exposed to intercellular air space per unit (one side) of leaf surface area (M index)	S_{mes}	$\mu m^2\ \mu m^{-2}$
Total mesophyll cell surface area occupied by chloroplasts exposed to intercellular air space per unit (one side) of leaf surface area (chloroplast index)	S_{chl}	$\mu m^2\ \mu m^{-2}$
M cell structural traits		
Area of cell section (in a leaf cross section)	a_{cell}	μm^2
Ratio between perimeter and area of a cell section (in a leaf cross section)	P/a_{cell}	$\mu m\ \mu m^{-2}$
Cell surface lobing (corresponding to cell perimeter tortuosity)	Lob_{cell}	$\mu m\ \mu m^{-1}$
Cell wall thickness	$Thick_{cw}$	μm
Length of a single cell wall exposed to intercellular air space	L_{cw_IAS}	μm
Fraction of cell wall exposed to intercellular air space	CW_{IAS}	%
Length of a single cell wall exposed to intercellular air space covered by chloroplasts	$L_{cw\_IAS\_chl}$	μm
Fraction of cell wall exposed to intercellular air space covered by chloroplasts	CW_{IAS_chl}	%
Length of a single cell wall adjacent to other cells	L_{ACW}	μm
Length of a single cell wall adjacent to other cells covered by chloroplasts	L_{ACW_chl}	μm
Fraction of cell wall adjacent to other cells covered by chloroplasts	ACW_{chl}	%
Fraction of cell wall covered by chloroplasts	CW_{chl}	%
Fraction of cell volume occupied by chloroplasts	Vol_{chl}	%
Fraction of cell volume occupied by vacuole	Vol_{vac}	%
Mitochondria minor axis	d_{mit}	μm
Leaf functional traits		
$^{13}C/^{12}C$ biomass isotopic signature	$\delta^{13}C$	‰
Maximum net photosynthetic rate per unit (one side) of leaf surface area	A_{max}	$\mu mol\ CO_2\ m^{-2}\ s^{-1}$
Maximum carboxylation efficiency	CE	$mol\ CO_2\ m^{-2}\ s^{-1}\ bar^{-1}\ CO_2$
Mesophyll conductance to CO_2 diffusion	g_m[a]	$mol\ CO_2\ m^{-2}\ s^{-1}\ bar^{-1}\ CO_2$
Mesophyll resistance to CO_2 diffusion per unit of cell surface area exposed to intercellular air space	S_{mes}/g_m	$m^2\ s\ bar\ CO_2\ mol^{-1}\ CO_2$
CO_2 compensation point at 20% oxygen	Γ	μbar
Intercellular partial pressure of CO_2	C_i[a]	μbar
Difference between atmospheric and intercellular partial pressure of CO_2	$C_a - C_i$[a]	μbar
Chloroplastic partial pressure of CO_2	C_c[a]	μbar
Difference between intercellular and chloroplastic partial pressure of CO_2	$C_i - C_c$[a]	μbar
Stomatal conductance to water vapor diffusion	g_{s_H2O}[a]	$mol\ water\ m^{-2}\ s^{-1}$
Stomatal conductance to CO_2 diffusion	g_{s_CO2}[a]	$mol\ CO_2\ m^{-2}\ s^{-1}$
Ratio between mesophyll and stomatal conductance to CO_2 diffusion	g_m/g_{s_CO2}	bar^{-1}
Net photosynthetic rate per unit (one side) of leaf surface area	A[a]	$\mu mol\ CO_2\ m^{-2}\ s^{-1}$
Transpiration rate per unit (one side) of leaf surface area	E[a]	$mmol\ water\ m^{-2}\ s^{-1}$
Transpiration efficiency	A/E	$\mu mol\ CO_2\ mmol^{-1}\ water$
Intrinsic transpiration efficiency	A/g_{s_H2O}	$\mu mol\ CO_2\ mol^{-1}\ water$

[a]Determined at 350 μbar air partial pressure of CO_2.

from 35% to 56%, and the fraction of M cell wall exposed to IAS covered by chloroplasts (CW_{IAS_chl}) ranged from 64% to 98%. The fraction of cell wall adjacent to other cells (ACW) and ACW covered by chloroplasts (ACW_{chl}) varied from 69% in *O. latifolia* 18, to 93% in *O. nivara*. There was a 5.3-fold difference in the fraction of cell volume occupied by vacuoles; it was lowest in *O. rufipogon* 9 (8.2%; Fig. 1, E and F), medium high in *O. coarctata* (Fig. 1, N and O), and highest in *O. glaberrima* (43.3%).

There is an approximately 4-fold difference in the leaf cumulative stomatal pore area index (I_{st}), which is lowest in *Oryza alta* (having low stomatal density and size) and highest in *O. barthii* (having high stomatal density and size). In general, except for *O. coarctata* and *O. brachyantha*, the stomatal density

Table III. *Overall significance of three-stage (genomes, species, accessions) nested ANOVA for all considered leaf structural and functional traits in the genus Oryza*

Trait symbols correspond to the descriptions in Table II. Asterisks represent the significance for differences among genomes, species nested within genomes, and accessions nested within species and genomes. $*P < 0.05$, $**0.01 \geq P \geq 0.001$, $***P < 0.001$. Min and Max correspond to the minimum and maximum means. F = F test statistic; Num df and Den df = numerator and denominator degrees of freedom, respectively.

Trait Category/Trait	Unit	Min	Max	Genomes						Species						Accessions			
				F	Num df	Den df	*P*	Min	Max	*F*	Num df	Den df	*P*	Min	Max	*F*	Num df	Den df	*P*
Leaf and cell structural																			
D_{st} ab	mm^{-2}	156.8	391.2	8.63	7	39	***	156.8	450.0	4.25	9	39	***	156.8	450.0	1.10	3	39	
D_{st} ad	mm^{-2}	167.3	501.0	11.61	7	38	***	147.3	501.0	2.09	9	38		147.3	501.0	0.67	3	38	
L_{st} ab	μm	9.67	17.32	14.67	7	39	***	8.87	18.07	9.54	9	39	***	8.87	19.03	0.91	3	39	**
L_{st} ad	μm	10.50	17.67	6.42	7	39	***	10.1	17.67	2.11	9	39		10.1	18.57	0.99	3	39	
I_{st} ab	$mm^2\ mm^{-2}$	0.028	0.062	5.47	7	39	***	0.017	0.091	4.82	9	39	***	0.017	0.099	5.87	3	39	**
I_{st} ad	$mm^2\ mm^{-2}$	0.009	0.012	8.89	7	38	***	0.026	0.140	1.49	9	38		0.026	0.140	0.75	3	38	
I_{st}	$mm^2\ mm^{-2}$	0.183	0.062	7.03	7	38	***	0.043	0.183	3.53	9	38	**	0.043	0.183	3.10	3	38	*
$Thick_{leaf}$	μm	57.8	120.4	26.02	7	28	***	57.8	120.4	6.98	9	28	***	57.8	125.3	1.44	1	28	
Vol_{IAS}	%	15.75	25.70	4.59	7	28	**	15.75	25.97	2.20	9	28		15.75	27.95	2.13	1	28	
S_{mes}	$\mu m\ \mu m^{-2}$	10.17	24.43	15.71	7	28	***	8.77	24.43	4.25	9	28	**	8.77	24.43	0.04	1	28	
S_{chl}	$\mu m\ \mu m^{-2}$	9.05	23.40	22.98	7	28	***	6.27	23.40	6.15	9	28	***	7.90	23.40	3.42	1	28	
a_{cell}	μm^2	58.8	208.2	7.29	7	19	***	58.8	242.6	2.14	9	19		58.8	242.6	0.11	1	19	
P/a_{cell}	$\mu m\ \mu m^{-2}$	0.380	0.580	4.62	7	19	**	0.380	0.590	1.58	9	19		0.370	0.590	0.12	1	19	
Lob_{cell}	$\mu m\ \mu m^{-1}$	1.218	1.403	8.83	7	19	***	1.060	1.445	1.32	9	19		1.060	1.445	0.01	1	19	
$Thick_{cw}$	μm	0.150	0.190	3.43	7	20	*	0.125	0.190	5.55	9	20	***	0.125	0.190	6.87	1	20	*
L_{cw_IAS}	μm	14.60	40.78	7.41	7	20	***	14.60	41.20	2.24	9	20		14.60	41.20	0.00	1	20	
CW_{IAS}	%	38.0	54.8	8.21	7	20	***	35.0	54.8	2.50	9	20	*	35.0	55.5	0.16	1	20	
$L_{cw\_IAS\_chl}$	μm	13.15	39.58	9.53	7	20	***	13.15	39.58	2.00	9	20		13.15	39.80	0.01	1	20	
CW_{IAS_chl}	%	86.55	97.13	1.69	7	20		63.75	97.95	3.63	9	20	**	63.75	97.95	0.01	1	20	
L_{ACW}	μm	16.60	50.63	5.95	7	20	***	16.60	52.30	1.24	9	20		16.60	52.30	0.09	1	20	
L_{ACW_chl}	μm	14.15	36.10	3.82	7	20	**	14.15	38.20	0.95	9	20		14.15	38.20	0.01	1	20	
ACW_{chl}	%	72.23	88.56	4.54	7	20	**	68.85	93.05	1.95	9	20		68.85	93.05	0.60	1	20	
CW_{chl}	%	78.37	91.56	3.07	7	20	*	73.95	94.30	2.53	9	20	*	73.95	94.30	0.05	1	20	
Vol_{chl}	%	49.85	61.68	2.09	7	20		39.00	64.45	3.84	9	20		39.00	64.45	0.28	1	20	
Vol_{vac}	%	15.30	27.35	2.23	7	20		8.20	43.25	6.63	9	20	***	8.20	43.25	0.11	1	20	
d_{mit}	μm	0.475	0.745	6.49	7	20	***	0.385	0.745	4.38	9	20	**	0.385	0.755	0.10	1	20	
Leaf functional																			
$\delta^{13}C$	‰	−26.86	−24.03	13.18	7	43	***	−27.37	−24.03	4.92	9	43	***	−27.42	−24.03	2.38	6	43	*
A_{max}	$\mu mol\ CO_2\ m^{-2}\ s^{-1}$	29.40	45.27					24.47	45.27					24.22	46.56				
CE	$mol\ CO_2\ m^{-2}\ s^{-1}\ bar^{-1}\ CO_2$	0.044	0.189	11.64	7	47	***	0.044	0.189	5.61	9	46	***	0.044	0.202	3.00	7	46	**
g_m	$mol\ CO_2\ m^{-2}\ s^{-1}\ bar^{-1}\ CO_2$	0.051	0.467	19.94	7	46	***	0.051	0.467	5.05	9	46	***	0.051	0.555	9.38	7	46	***
S_{mes}/g_m	$m^2\ s\ bar\ CO_2\ mol^{-1}\ CO_2$	21.9	337.2	20.08	7	27	***	21.9	337.2	1.52	9	27		21.9	337.2	0.55	1	27	
Γ	μbar	40.55	52.92	11.58	7	48	***	37.17	52.92	2.38	9	48	*	37.17	52.92	2.58	7	48	*
C_i	μbar	219.7	278.4	4.65	7	47	**	219.7	278.4	1.78	9	47		208.7	278.4	0.71	7	47	
$C_a - C_i$	μbar	75.6	134.3	4.65	7	47	**	75.6	134.3	1.75	9	47		75.6	145.3	0.79	7	47	
C_c	μbar	89.1	178.4	7.32	7	41	***	89.1	185.4	2.28	9	41	*	89.1	188.0	1.91	7	41	
$C_i - C_c$	μbar	45.5	145.4	13.74	7	41	***	45.5	145.4	3.37	9	41	*	40.5	145.4	2.05	7	41	
g_{s_H2O}	$mol\ water\ m^{-2}\ s^{-1}$	0.13	0.417	4.39	7	45	**	0.13	0.520	1.38	9	45		0.13	0.572	1.67	7	45	
g_m/g_{s_CO2}	bar^{-1}	0.619	2.566	5.87	7	43	***	0.619	2.566	0.93	9	43		0.619	3.369	2.84	7	43	
A	$\mu mol\ CO_2\ m^{-2}\ s^{-1}$	9.65	22.87	11.67	7	47	***	9.65	27.09	3.39	9	47	**	9.65	27.09	2.76	7	47	*
E	$mmol\ water\ m^{-2}\ s^{-1}$	2.40	6.08	4.00	7	45	**	2.40	7.74	1.88	9	45		2.40	7.81	3.06	7	45	*
A/E	$\mu mol\ CO_2\ mmol^{-1}\ water$	2.85	4.49	1.42	7	45		2.85	4.69	1.97	9	45		2.85	5.40	4.05	7	45	**
A/g_{s_H2O}	$\mu mol\ CO_2\ mol^{-1}\ water$	51.45	80.64	2.68	7	45	*	41.10	80.64	2.69	9	45	*	41.10	80.64	0.85	7	45	

is higher on the abaxial than on the adaxial lamina surface.

Differences in Leaf Functional Traits across Accessions

The minimum and maximum means within *Oryza* accessions for each leaf functional trait, are shown in Table III (for mean trait values for each accession, see Supplemental Table S3). The difference in A was approximately 2.9-fold (minimum of 9.7 μmol CO_2 m^{-2} s^{-1} in *O. brachyantha* and maximum of 27.1 μmol CO_2 m^{-2} s^{-1} in *O. glaberrima*), that in E was approximately 3-fold, and that in A/E and intrinsic transpiration efficiency (A/g_{s_H2O} ratio) was approximately 2-fold. The difference in CE was approximately 4.6 fold (minimum in *O. brachyantha* and maximum in *O. australiensis* 22), in g_m was approximately 10.9 fold (maximum in *O. australiensis* 21, minimum in *O. coarctata*), and in M resistance to CO_2 per unit of cell surface area exposed to IAS (S_{mes}/g_m) was approximately 15-fold. In addition, across accessions, there was a range of approximately 1.4-fold in CO_2 compensation point (Γ), approximately 1.3-fold in C_i, and approximately 2-fold in C_c. There was an approximately 4.4-fold difference in g_{s_H2O} and an approximately 5.4-fold difference in the ratio between g_m and g_{s_CO2}.

Leaf Structural-Functional Principal Factor Analysis

From principal factor analysis (PFA) performed on the leaf structural and functional traits of *Oryza* accessions four main axes of covariation (factors) were considered (for trait loadings on the factors, see Fig. 2, left side). The cluster of interrelated leaf traits with high positive association with factor 1 included $Thick_{leaf}$ (along with other structural features, Vol_{IAS}, S_{mes}, S_{chl}, and a_{cell}), maximum net photosynthetic rate (A_{max}), and A/E; A/g_{s_H2O} had a lower positive association. In contrast, E and the ratio between M cell perimeter and cell section area in a leaf cross section (P/a_{cell}) had negative associations. Factor 1 was interpreted to represent M architecture. The cluster of interrelated leaf traits with high positive associations with factor 2 included A, CE, g_m, C_c, g_{s_H2O}, and E, while g_m/g_{s_CO2} had a lower positive linkage; conversely, the difference between intercellular and chloroplastic partial pressure of CO_2 ($C_i - C_c$) and S_{mes}/g_m had negative associations with factor 2 (Fig. 2, left side). Factor 2 was interpreted to represent photosynthetic-transpiration activity. Factors 1 and 2 accounted for 27.1% and 19.6% of the total variability, respectively.

A third cluster of interrelated leaf traits positively associated with factor 3 included stomatal density in both the abaxial ($D_{st}ab$) and adaxial ($D_{st}ad$) lamina surfaces, $I_{st}ab$ and stomatal pore area index in the adaxial lamina surface ($I_{st}ad$), leaf cumulative I_{st}, and ACW_{chl}, while Vol_{IAS} had a negative linkage. Factor 3 was interpreted to represent leaf stomatal composition; it accounted for 13.0% of total variability (Fig. 2, left side; data not shown). The fourth cluster of interrelated leaf traits positively associated with factor 4 included CW_{IAS_chl}, ACW_{chl}, CW_{chl}, and the fraction of cell volume occupied by chloroplasts (Vol_{chl}), while the fraction of cell volume occupied by vacuole (Vol_{vac}) had a negative loading. Factor 4 was taken to represent M cell chloroplast display; it accounted for 12.0% of the total variability (Fig. 2, left side; data not shown). In total, the main four factors accounted for 71.7% of the total variability in the data set.

The *Oryza* accessions loaded on M architecture (factor 1) and photosynthetic-transpiration activity (factor 2) are shown in Figure 2, right side (the corresponding scores are displayed in Supplemental Table S4, right side). In general, the accessions tended to group in three clusters based on M architecture, while they showed an overall higher variability on photosynthetic-transpiration activity. In particular, *O. australiensis* 20 and 21 and *O. rhizomatis* 16 had high scores on factor 1, while *O. rufipogon* 9 and *O. glumaepatula* 3 had low scores on this factor. However, all these species had high scores on factor 2. The rice accessions *O. sativa* cv IR64 (10) and *O. glaberrima* 2 had the highest scores on factor 2; vice versa, *O. brachyantha* 23 and *O. coarctata* 24 had the lowest scores (but *O. coarctata* had high scores on factor 1 compared with *O. brachyantha* 23). The accession scores for factor 3 and 4 are not graphed but are displayed in Supplemental Table S4, right side.

Pearson Correlation Matrices for Structural, Functional, and Structural-Functional Leaf Traits

To complement the PFA, trait-to-trait correlations were further analyzed, based on the data set. The Pearson correlation matrix for leaf structural traits is shown in Supplemental Table S5. In particular, $Thick_{leaf}$ showed positive correlations with several leaf structural features, including a_{cell}, S_{mes}, S_{chl} ($P < 0.01$), and Vol_{IAS} ($P < 0.05$). S_{mes} and S_{chl} are highly correlated ($r = 0.97$; $P < 0.01$). S_{mes} was also closely associated with $I_{st}ad$ ($r = 0.67$; $P < 0.01$). Lob_{cell} showed a positive correlation with the length of M cell walls adjacent to other cells covered by chloroplasts (L_{ACW_chl}; $P < 0.01$), and also with a_{cell}, although not significant ($r = 0.30$). There was a close negative association between Vol_{chl} and Vol_{vac} ($P < 0.01$).

The Pearson correlation matrix for leaf functional traits is shown in Supplemental Table S6. There is a positive correlation between CE and both A and A_{max} ($P < 0.01$). g_m has a positive association with A and C_c ($P < 0.01$) and with g_{s_H2O} ($P < 0.05$). g_m was negatively correlated ($P < 0.01$) with S_{mes}/g_m, which is linked to the large difference in g_m across accessions compared with S_{mes}. S_{mes}/g_m exhibited a negative association with C_c, g_{s_H2O}, A, and E ($P < 0.01$) and with CE ($P < 0.05$). C_i was negatively associated with A/g_{s_H2O}, A/E, and g_m/g_{s_CO2} ($P < 0.01$). There was a tight positive correlation between A and E ($P < 0.01$). In addition, g_{s_H2O} was positively correlated with both A and E and negatively associated with $C_i - C_c$ ($P < 0.01$).

Eigenvalue	11.36	8.25	5.46	5.05
Var_{tot} expl (%)	27.05	19.63	13	12.02
Trait	**Factor 1**	**Factor 2**	**Factor 3**	**Factor 4**
D_{st} ab	-0.25	**0.59**	**0.48**	-0.08
D_{st} ad	-0.08	-0.26	**0.87**	0.02
L_{st} ab	**0.40**	-0.13	0.00	0.06
L_{st} ad	**0.43**	-0.07	-0.01	-0.20
I_{st} ab	0.03	**0.60**	**0.55**	-0.21
I_{st} ad	0.14	-0.35	**0.85**	-0.11
I_{st}	0.06	0.06	**0.94**	-0.23
$Thick_{leaf}$	**0.93**	-0.10	-0.02	0.07
Vol_{IAS}	**0.49**	-0.06	**-0.41**	0.17
S_{mes}	**0.72**	-0.38	**0.42**	0.23
S_{chl}	**0.70**	-0.39	0.34	0.38
a_{cell}	**0.70**	0.01	-0.39	-0.23
P/a_{cell}	**-0.66**	0.06	**0.43**	0.24
Lob_{cell}	-0.01	0.12	0.12	-0.13
$Thick_{cw}$	0.22	-0.31	-0.01	-0.04
L_{CW_IAS}	**0.85**	-0.03	-0.06	-0.01
CW_{IAS}	**0.72**	-0.09	0.24	0.27
$L_{CW\_IAS\_chl}$	**0.81**	-0.08	-0.13	0.26
CW_{IAS_chl}	0.09	-0.21	-0.25	**0.87**
L_{ACW}	0.17	0.03	-0.36	-0.39
L_{ACW_chl}	0.20	0.18	-0.16	-0.21
ACW_{chl}	-0.01	0.21	**0.54**	**0.68**
CW_{chl}	0.13	0.02	0.21	**0.94**
Vol_{chl}	0.12	0.03	-0.31	**0.85**
Vol_{vac}	0.05	-0.03	0.23	**-0.92**
d_{mit}	**0.62**	-0.01	**-0.46**	0.09
$\delta^{13}C$	0.10	-0.39	-0.05	-0.05
A_{max}	**0.79**	0.28	0.02	-0.12
CE	**0.50**	**0.72**	0.04	-0.13
g_m	-0.03	**0.83**	-0.06	0.19
Γ	-0.15	-0.21	-0.13	-0.05
C_i	**-0.45**	-0.11	-0.09	-0.08
C_a-C_i	**0.45**	0.11	0.09	0.08
C_c	0.01	**0.87**	-0.13	-0.17
C_i-C_c	-0.13	**-0.89**	0.08	-0.14
g_{s_H2O}	-0.27	**0.81**	0.02	0.13
g_m/g_{s_CO2}	0.19	**0.53**	-0.19	0.12
S_{mes}/g_m	0.17	**-0.84**	**0.45**	-0.01
A	0.03	**0.95**	0.08	-0.09
E	**-0.46**	**0.78**	-0.04	-0.02
A/E	**0.78**	0.15	0.18	-0.05
A/g_{s_H2O}	**0.47**	-0.15	0.18	-0.28

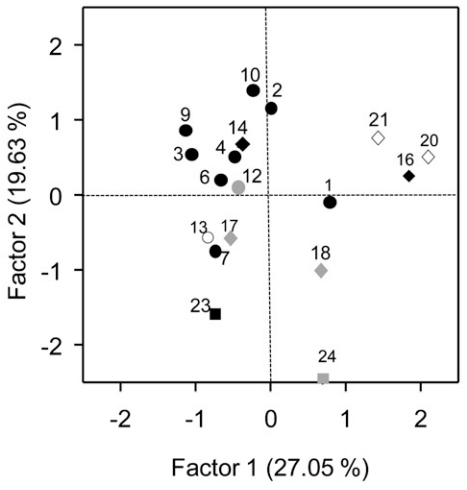

Genome	Specie	Accession Number
AA	*O. barthii*	1
AA	*O. glaberrima*	2
AA	*O. glumaepatula*	3
AA	*O. longistaminata*	4
AA	*O. longistaminata*	
AA	*O. meridionalis*	6
AA	*O. nivara*	7
AA	*O. rufipogon*	
AA	*O. rufipogon*	9
AA	*O. sativa*	10
AA	*O. sativa*	
BB	*O. punctata*	12
BBCC	*O. minuta*	13
CC	*O. officinalis*	14
CC	*O. rhizomatis*	
CC	*O. rhizomatis*	16
CCDD	*O. alta*	17
CCDD	*O. latifolia*	18
CCDD	*O. latifolia*	
EE	*O. australiensis*	20
EE	*O. australiensis*	21
EE	*O. australiensis*	
FF	*O. brachyantha*	23
HHKK	*O. coarctata*	24

Figure 2. PFA of leaf structural and functional traits. At left are factor loadings for all leaf structural and functional traits determined on 18 *Oryza* accessions. Var_{tot} expl, Total variance explained. Factor loadings greater than 0.4 in absolute value are shown in boldface. The graph associated with the data are in Supplemental Table S4, left side. Trait symbols are as in Table II. At right are loadings of the *Oryza* accessions (identified by number as in Table I) on factor 1 (M architecture) and factor 2 (photosynthetic-transpiration activity). Genome symbols are associated with each accession.

The portion of the Pearson correlation matrix showing the leaf structural-functional trait-to-trait associations is in Supplemental Table S7. $Thick_{leaf}$ had a close negative correlation with C_i ($P < 0.01$) and a positive association with A_{max} ($P < 0.01$); it had a negative relationship with E ($P > 0.05$) and significant positive associations with A/E ($P < 0.01$) and A/g_{s_H2O} ($P < 0.05$). In addition, S_{mes} had a tight negative association with E ($P < 0.01$) and close positive associations with A/E ($P < 0.01$) and A/g_{s_H2O} ($P < 0.05$).

With respect to stomatal traits on the abaxial leaf surface, D_{st}ab has a significant positive association with g_{s_H2O} ($P < 0.05$) and with A and E ($P < 0.01$); in addition, I_{st}ab has a positive association with CE ($P < 0.05$) and a negative strong relationship with $\delta^{13}C$ ($P < 0.01$). In contrast, on the adaxial leaf surface, there is a significant positive correlation between I_{st}ad and S_{mes}/g_m ($P < 0.01$). In addition, I_{st}ad has a negative association with E ($r = -0.41$; $P > 0.05$) and a positive association with A/g_{s_H2O} ($P < 0.05$). Lob_{cell} has a negative correlation with Γ ($P < 0.05$). Although not significant ($P > 0.05$), the results suggest that $Thick_{cw}$ has a negative relationship with g_m ($r = -0.42$) and a positive association with S_{mes}/g_m ($r = 0.37$).

Trait-to-Trait Correlations

Considering the clusters of interrelated leaf traits closely associated with PFA factors 1 and 2, and of parameters of most interest with respect to relationships between leaf structure, photosynthesis, and transpiration (see introduction), trait-to-trait correlations were analyzed in plots of mean values for each *Oryza* accession (Figs. 3–10; note that in most panels, the Pearson correlation coefficients were significant; Supplemental Tables S5–S7).

Structural Traits

First, with respect to structural traits, the significant positive associations between mean values of Vol_{IAS}, S_{mes}, and a_{cell}, and the corresponding mean values of $Thick_{leaf}$, are shown in Figure 3. In particular, *O. australiensis* 20 and 21, *O. rhizomatis* 16, and *O. coarctata* 24 showed the highest values for these M and cell structural features. In contrast, *O. brachyantha* 23 and *O. sativa* cv IR64 (10) had the lowest values. There is also a close positive association between Lob_{cell} and L_{ACW_chl} (Fig. 4), which is in part driven by *O. brachyantha* 23, which has the lowest L_{ACW_chl} value; *O. barthii* 1 has the highest L_{ACW_chl} value.

Functional Traits

Significant relationships for leaf functional features associated with the photosynthetic process are shown in Figures 5 and 6. In the close positive association between A and g_{s_CO2} across accessions (Fig. 5A), *O. coarctata* 24 and *O. brachyantha* 23 have the lowest values for both traits; in contrast, *O. sativa* cv IR64 (10) and *O. latifolia* 19 have the highest A (above 25 μmol CO_2 m^{-2} s^{-1}) and g_{s_CO2} values. There is also a strong positive association between A and g_m (Fig. 5B); however, there were deviations; *O. australiensis* 21 and 22 have the highest g_m values (close to 0.55 mol CO_2 m^{-2} s^{-1} bar^{-1} CO_2) but not the highest A. Also, very high g_m values (greater than 0.45 mol CO_2 m^{-2} s^{-1} bar^{-1} CO_2) were found in *O. rufipogon* 9, with A approximately 25 μmol CO_2 m^{-2} s^{-1}, and in *Oryza punctata* 12, with A approximately 22 μmol CO_2 m^{-2} s^{-1}. In the plot of g_m versus g_{s_CO2} (Fig. 5C), there is no apparent linear relationship; rather, two pools of data are recognized. In particular, there is a close positive relationship between g_m and g_{s_CO2} up to g_m values of 0.35 mol CO_2 m^{-2} s^{-1} bar^{-1} CO_2 ($r = 0.78$; $P < 0.01$). At the higher g_m values, from 0.35 up to 0.56 mol CO_2 m^{-2} s^{-1} bar^{-1} CO_2, there is a negative relationship between g_m and g_{s_CO2} ($r = -0.64$; $P > 0.05$), notably in *O. australiensis* 21 and 22, *O. rufipogon* 9, *O. punctata* 12, *O. latifolia* 19, *O. glaberrima* 2, *Oryza longistaminata* 4, and *O. meridionalis* 6. Figure 6 shows the significant negative correlation between C_c and S_{mes}/g_m, which is partially driven by the high S_{mes}/g_m values of *O. coarctata* 24 and *O. brachyantha* 23 (above 180 m^2 s bar CO_2 mol^{-1} CO_2); most accessions have mean S_{mes}/g_m values in the range of 25 to 80 m^2 s bar CO_2 mol^{-1} CO_2.

Plots of important relationships between leaf functional features associated with transpiration are shown in Figure 7. In Figure 7A, the significant negative correlation between g_{s_H2O} and $C_i - C_c$ (which is partially driven by the highest $C_i - C_c$ and the lowest g_{s_H2O} values of *O. coarctata* 24 and *O. brachyantha* 23) reflects a significant negative association between E and $C_i - C_c$ (data not shown). *O. australiensis* 21 and 22, *O. rufipogon* 9, and *O. sativa* cv IR64 (10) had the lowest $C_i - C_c$ values; among these accessions, *O. australiensis* 21 also had a medium-low g_{s_H2O}. *O. glaberrima* 2, *O. latifolia* 19, and

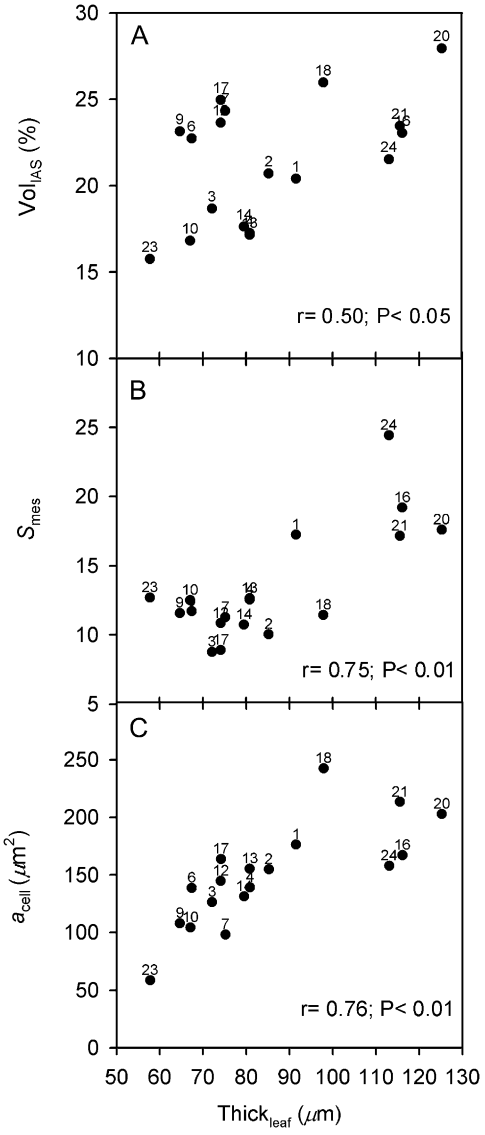

Figure 3. Correlation of leaf thickness with other leaf structural traits in *Oryza* accessions. A, Vol_{IAS}. B, S_{mes}. C, a_{cell}. Points are mean values per accession (SE values are given in Supplemental Table S3). Numbers correspond to the accessions listed in Table I.

O. australiensis 20 also had relatively low $C_i - C_c$ values. The tendency for a general positive association between $\delta^{13}C$ and A/g_{s_H2O} (i.e. less negative $\delta^{13}C$ tends to correspond to high A/g_{s_H2O}) is displayed in Figure 7B. In particular, *O. nivara* 7 has the lowest $\delta^{13}C$ (the most negative value) and the lowest A/g_{s_H2O}, while *O. punctata* 12 has the highest $\delta^{13}C$ and a medium A/g_{s_H2O} value. *O. australiensis* 21 and *O. glaberrima* 2 were outliers, as they have low $\delta^{13}C$ values (more negative than −26.7‰) and the highest A/g_{s_H2O} values.

Structural Versus Functional Traits

Important relationships between leaf structural and functional traits related to both photosynthesis and

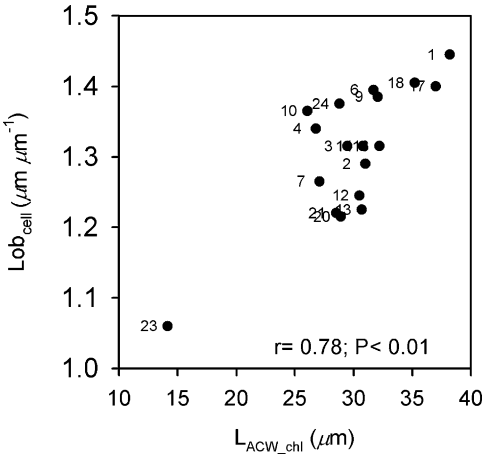

Figure 4. Correlation, across *Oryza* accessions between Lob_{cell} and L_{ACW_chl}. Points are mean values per accession (SE values are given in Supplemental Table S3). Numbers correspond to the accessions listed in Table I.

transpiration are shown in Figures 8–10. There is a significant positive association between $Thick_{leaf}$ and A_{max} (Fig. 8A), with *O. australiensis* 20 and 21 and *O. rhizomatis* 16 having the highest values for both traits. There is a close negative association between $Thick_{leaf}$ and C_i (Fig. 8B), with *O. australiensis* 21 and *O. coarctata* 24 having the lowest C_i values. Results suggestive of a negative association between $Thick_{leaf}$ and E are displayed in Figure 8C; *O. australiensis* 20 is an outlier, having high $Thick_{leaf}$ and a relatively high E, while *O. brachyantha* 23 is an outlier that has the lowest $Thick_{leaf}$ along with low E. Figure 8D shows the close positive association between $Thick_{leaf}$ and A/E; among accessions having the thickest leaves, *O. rhizomatis* 16 and *O. australiensis* 21 have the highest A/E values, while *O. australiensis* 20 is an outlier with a medium A/E value. Also, there is a significant positive association ($r = 0.59$; $P < 0.05$) between $Thick_{leaf}$ and A/g_{s_H2O} (data not shown).

The significant positive relationship between A and $D_{st}ab$ is shown in Figure 9. *O. coarctata* 24 has the lowest $D_{st}ab$, while *O. rufipogon* 9 has the highest value. *O. sativa* cv IR64 (10) and *O. glaberrima* 2 have medium to high $D_{st}ab$ and the highest A values.

The data suggestive of a positive association between $Thick_{cw}$ and M resistance to CO_2 diffusion per unit of cell surface area exposed to IAS are shown in Figure 10A. *O. coarctata* 24 and *O. brachyantha* 23 are outliers, with high S_{mes}/g_m values. Results suggestive of a negative correlation between $Thick_{cw}$ and g_m are shown in Figure 10B. In particular, accessions having g_m values greater than 0.45 mol CO_2 m^{-2} s^{-1} bar^{-1} CO_2 (including *O. rufipogon* 9, *O. punctata* 12, and *O. australiensis* 21) had $Thick_{cw}$ of 0.150 μm or less. All the accessions above the dashed line in Figure 10B correspond to those in Figure 10A having the lowest S_{mes}/g_m values and to those in Figure 5C having a negative association between g_m (for values above 0.35 mol CO_2 m^{-2} s^{-1} bar^{-1} CO_2) and g_{s_CO2}. In contrast, the accessions below the dashed line have the highest S_{mes}/g_m (Fig. 10A) and a positive correlation between g_m (below 0.35 mol CO_2 m^{-2} s^{-1} bar^{-1} CO_2) and g_{s_CO2} (Fig. 5C).

There is a negative association between Γ and Lob_{cell} (data not shown; $r = -0.53$; $P < 0.05$); this is driven in part by *O. brachyantha* 23, which has the highest Γ (52.9 μbar) and the lowest Lob_{cell} (1.060 μm μm^{-1}), and by *O. minuta* 13, which also has a high Γ (51.7 μbar) and Lob_{cell} of 1.225 μm μm^{-1} (Supplemental Table S3).

DISCUSSION

Interrelations among Leaf Thickness and Other Leaf Structural Traits

The hypothesis that in *Oryza* species some M structural traits will be associated with leaf thickness was

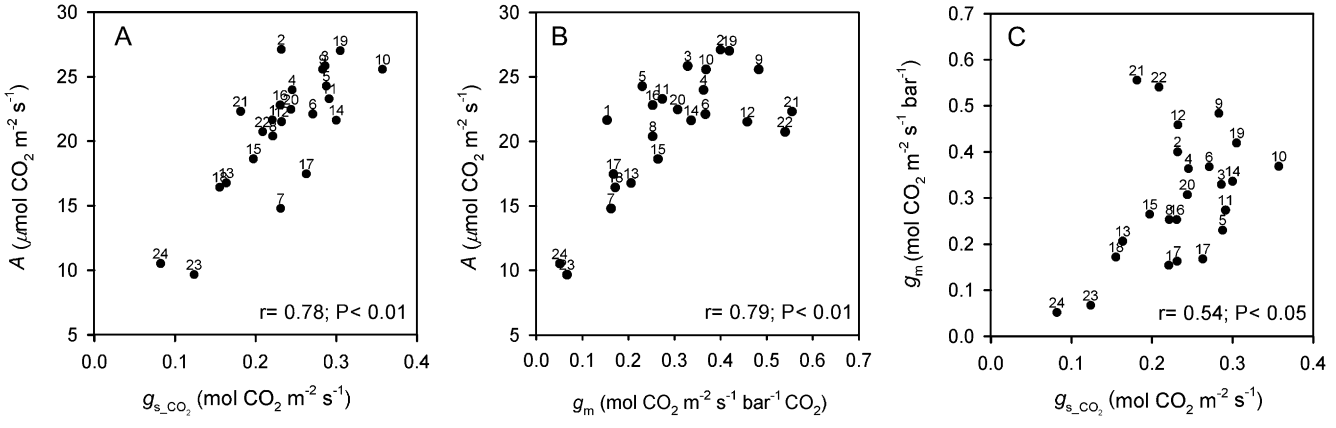

Figure 5. Correlations between leaf functional traits associated with the photosynthetic process in accessions of *Oryza* species. A, A versus stomatal conductance to CO_2 diffusion. B, A versus M conductance to CO_2 diffusion. C, g_m versus stomatal conductance to CO_2 diffusion. Points are mean values per accession (SE values are given in Supplemental Table S3). Numbers correspond to the accessions listed in Table I.

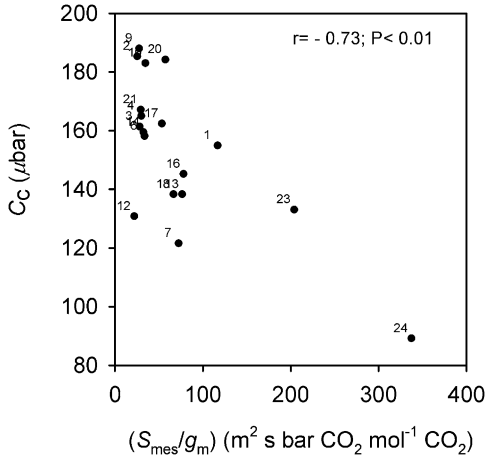

Figure 6. Correlation between C_c and S_{mes}/g_m across *Oryza* accessions. Points are mean values per accession (SE values are given in Supplemental Table S3). Numbers correspond to the accessions listed in Table I.

confirmed by the PFA results for factor 1 (M architecture) and by trait-to trait correlation analysis; in particular, $Thick_{leaf}$ had significant positive correlations with S_{mes} and S_{chl}, Vol_{IAS}, and a_{cell} (Terashima et al., 2006).

The positive correlation between $Thick_{leaf}$ and S_{mes} (and S_{chl}) suggests that the higher number of chloroplasts in thicker leaves is coordinated with increases in S_{mes}. In the absence of an association between $Thick_{leaf}$ and S_{mes}, more chloroplasts would become located away from the cell surface area facing the IAS: this would increase the M diffusive resistance to CO_2 (Nobel et al., 1975; Evans et al., 2009), and light availability for many chloroplasts could also become limited (Oguchi et al., 2003). In this regard, Hanba et al. (1999) found that the association between S_{mes} and $Thick_{leaf}$ holds across different leaf types among evergreen species.

A positive association was found across *Oryza* accessions between $Thick_{leaf}$ and Vol_{IAS}, with the mean $Thick_{leaf}$ ranging from approximately 58 to 125 μm and Vol_{IAS} from approximately 16% to 28%. Niinemets (1999), in a study on woody shrubs and grass species, reported a huge variation in leaf anatomy, with $Thick_{leaf}$ ranging from approximately 55 to 1,960 μm and M porosity (corresponding to Vol_{IAS} in this study) ranging from 10% to 36%. It was suggested that the variation in $Thick_{leaf}$ and in the corresponding leaf structural profile affects the pattern of light absorption through the layers of M cells and the distribution of chlorophyll and Rubisco, while the consequences for the diffusion of CO_2 in the IAS are considerably smaller.

In addition, in *Oryza* species, there was a tendency for a positive association between a_{cell} and Lob_{cell} (r = 0.30; $P > 0.05$); this suggests that Lob_{cell} may increase with cell volume, which could reduce the resistance to CO_2 diffusion into the larger M cells. Also, among *Oryza* accessions there is a tendency toward a positive association between $Thick_{cw}$ and both S_{mes} and $Thick_{leaf}$ (r = 0.42 and 0.24, respectively; $P > 0.05$); $Thick_{cw}$, acting as resistance in series for M CO_2 diffusion, may reduce g_m, as observed by Terashima et al. (2006).

Coordination between g_m and M Structural Traits

Another premise of this study was that g_m in *Oryza* accessions would be correlated with leaf M structural traits. Based on trait-to-trait analysis, g_m was not significantly correlated with any single M structural trait, including S_{mes}, Lob_{cell}, or $Thick_{cw}$; however, there was a tendency toward a lower g_m and higher S_{mes}/g_m with increasing M cell wall thickness ($P > 0.05$; Fig. 10). Lack of close correlations of g_m with single traits might be expected if there are covariations of multiple leaf and M cell structural traits that tend to have both positive (e.g. S_{mes}) and negative (e.g. $Thick_{cw}$) effects on g_m (Supplemental Materials and Methods S3; Terashima et al., 2011).

Based on the analysis conducted on leaf data from multiple species by Evans et al. (2009), there was an

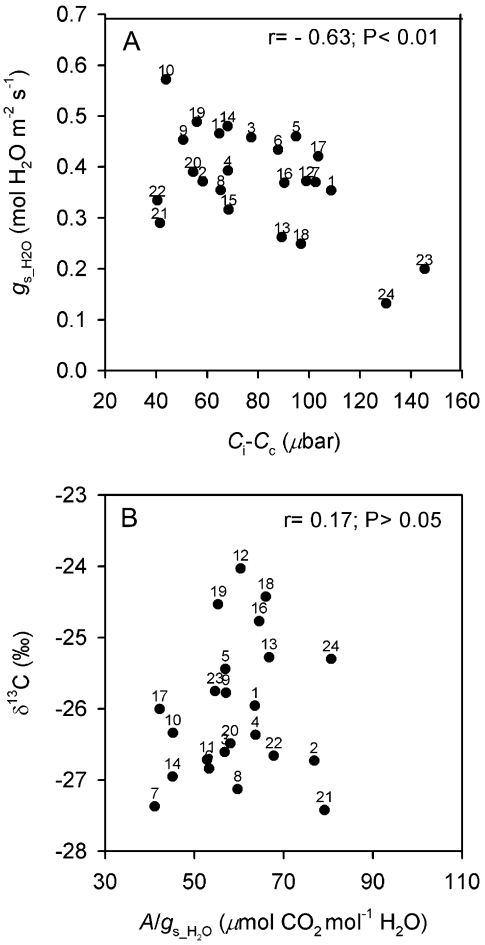

Figure 7. Correlations between leaf functional traits associated with the transpiration process in *Oryza* accessions. A, g_{s_H2O} and $C_i - C_c$. B, $\delta^{13}C$ and A/g_{s_H2O}. Points are mean values per accession (SE values are given in Supplemental Table S3). Numbers correspond to the accessions listed in Table I.

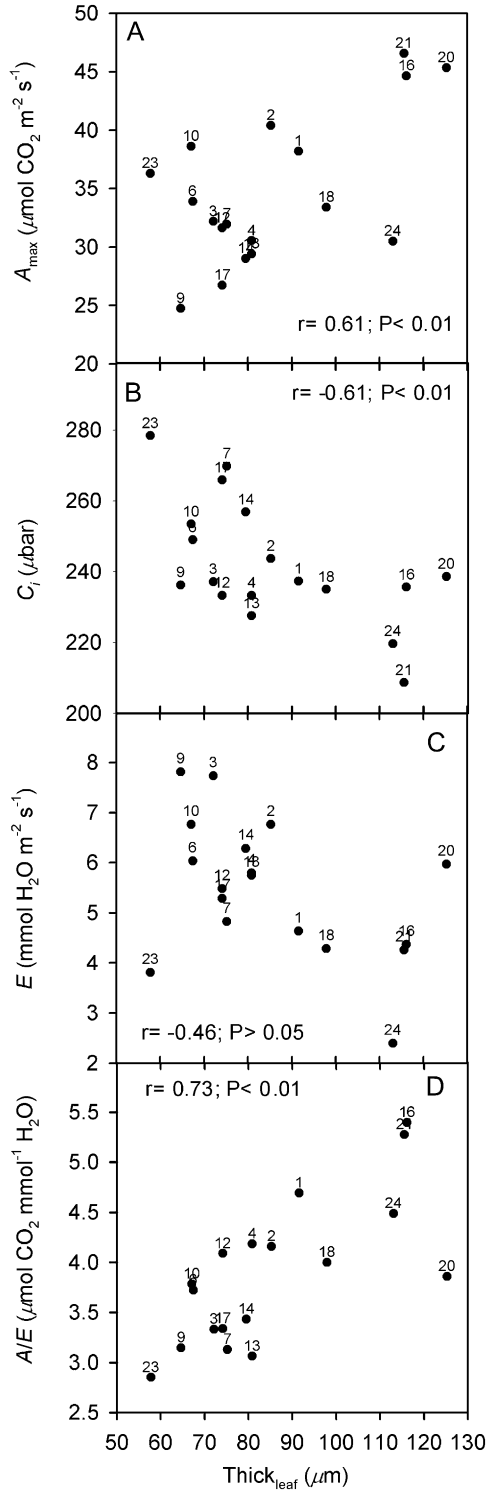

Figure 8. Correlations between $Thick_{leaf}$ and leaf functional traits in *Oryza* accessions. A, A_{max}. B, C_i. C, *E*. D, *A*/*E*. Points are mean values per accession (SE values are given in Supplemental Table S3). Numbers correspond to the accessions listed in Table I.

apparent positive correlation between g_m and S_{chl}, but with a low slope when $Thick_{cw}$ was greater than 0.140 μm. Since $Thick_{cw}$ in *Oryza* accessions is also relatively high (approximately 0.125–0.190 μm), this may account for the lack of a positive correlation between g_m and S_{mes} (or S_{chl}). Evans et al. (2009) estimated that the cell wall may contribute from 25% to 30% or more of the total M resistance to CO_2, even if changes in one component of the conduction pathway may be countered by pleiotropic compensatory changes; these findings are in agreement with Barbour et al. (2010).

Interestingly, lobes in M cells can increase the M cell surface to cell volume (Parker and Ford, 1982; Burundukova et al., 2003), which is convenient for CO_2 diffusion into the cell (Nobel, 2009), and they may contribute to S_{mes} (Nobel, 2009) and g_m (Evans and Loreto, 2000; Evans et al., 2009). M cell lobes are prominent in some *Oryza* species, and most lobes of contiguous cells do not interlock. Approximately 50% of the M cell wall is adjacent to other cells, with a high percentage of this area also occupied by chloroplasts. In contrast, C_3 species with high photosynthetic activity generally have few chloroplasts located where the cell wall is in contact with other cells (Evans et al., 2004). In *Oryza* accessions Lob_{cell} was positively correlated with the length of the cell wall adjacent to another cell (L_{ACW}) and with L_{ACW_chl}. These tight associations suggest that cell lobing may allow a larger proportion of the cell wall to be adjacent to other cells, while allowing for CO_2 and light access to the chloroplasts via the cell walls between the lobes. These M cell structural features may contribute to an increase in g_m and enhance leaf photosynthetic activity, with a positive feedback on the refixation of photorespired CO_2 (Nobel, 2009); this could lower Γ by decreasing the CO_2 chloroplastic photocompensation point. In this study, in fact, there was a significant negative association between Lob_{cell} and Γ ($P < 0.05$), and the results are also suggestive of a positive association between Lob_{cell} and A ($P > 0.05$). M cell lobes may be particularly beneficial in hot environments, where rates of photorespiration are high (Peterhansel and Maurino, 2011). Also, the relative positions of mitochondria and peroxisomes compared with chloroplasts in lobed M cells (Fig. 1; Sage and Sage, 2009) may enhance CO_2 refixation (Busch et al., 2013).

In addition to these leaf and M cell structural traits, the composition of cell walls, plasma membrane, and chloroplast envelope (Kogami et al., 2001; Nobel, 2009) as well as biochemical factors increasing membrane permeability to CO_2 are recognized to affect the CO_2 diffusion from IAS to chloroplast stroma (Bernacchi et al., 2002; Terashima and Ono, 2002; Terashima et al., 2006; Uehlein et al., 2008; Evans et al., 2009; Tosens et al., 2012). According to Flexas et al. (2007), the implication of active transport of CO_2 by cooporins in the regulation of g_m (Hanba et al., 2004; Flexas et al., 2006) may explain the weak relationship between g_m and leaf M structure. In this study, intrinsic differences in biochemical factors might partially explain the variation in S_{mes}/g_m among *Oryza* accessions.

No correlation was found across *Oryza* accessions between Vol_{IAS} and g_m, which might be explained by

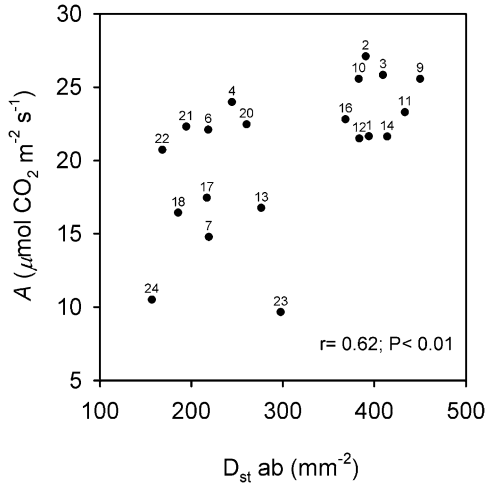

Figure 9. Correlation in *Oryza* accessions between leaf *A* and D_{st} ab. Points are mean values per accession (SE values are given in Supplemental Table S3). Numbers correspond to the accessions listed in Table I.

the fact that changes in the gaseous CO_2 diffusion resistances to variation in Vol_{IAS} tend to be relatively small (Niinemets, 1999; Nobel, 2009). Both negative and positive correlations between M porosity (corresponding to Vol_{IAS}) and g_m have been observed in previous studies (Flexas et al., 2008); this might depend on the covariation of some other structural trait that affects the resistance in the liquid phase and, consequently, g_m (Evans et al., 2009; Nobel, 2009). Several studies have shown that leaf density (g m^{-3}), leaf thickness, and their product leaf dry mass per unit (one side) of the leaf surface area (g m^{-2}) tend to be negatively linked to g_m and may set an upper limit for the maximum value of g_m (Terashima et al., 2006; Flexas et al., 2008; Niinemets et al., 2009). In particular, high leaf dry mass may be associated with thick leaves having thick M cell walls, which could offset the positive effect of S_{mes} on g_m and could contribute to an increase in the M resistance to CO_2 diffusion (Evans and von Caemmerer, 1996; Niinemets, 1999). Controversial results were found among evergreen, deciduous, and annual species in these relationships (Hanba et al., 1999).

Coordination between Functional Traits: *A*, g_s and g_m, and *E*

The hypothesis of correlations between *A*, g_s and g_m, and *E* in *Oryza* species was supported by the PFA results for factor 2 (photosynthesis-transpiration activity) and by trait-to-trait correlation analysis. The data indicate a coupling between photosynthesis and transpiration processes and are aligned with evidence that both g_s and g_m are important physical determinants of the CO_2 supply from the atmosphere to the chloroplasts (Evans and von Caemmerer, 1996; Evans, 1999; Evans and Loreto, 2000; Barbour et al., 2010).

However, across *Oryza* accessions despite an overall positive correlation between g_{s_CO2} and g_m ($P < 0.05$), a strong positive relationship ($P < 0.01$) between g_{s_CO2} and g_m up to g_m values of approximately 0.35 mol CO_2 m^{-2} s^{-1} bar^{-1} CO_2 was observed, corresponding to g_m/g_{s_CO2} ratios from 0.62 to approximately 1.4 bar^{-1}. Above this g_m threshold, there was a negative correlation ($P > 0.05$) between g_m and g_{s_CO2}, with g_m/g_{s_CO2} ratios between approximately 1.0 and 3.4 bar^{-1}. The contrasting relationships between g_m and g_s in the two g_m ranges have important implications for A/E in the different accessions. A meta-analysis of data from a multitude of grass, shrub, and tree species (Niinemets et al. (2009) revealed how photosynthesis tends to become more sensitive to fluctuations in stomatal conductance than in M conductance at high g_m values (or under conditions where g_m is higher than g_s). Similarly, in *Oryza* accessions the low sensitivity of *A* to changes in g_m higher than 0.35 mol CO_2 m^{-2} s^{-1} bar^{-1} CO_2 could be associated with a redistribution of overall CO_2 diffusion limitation between stomata (g_s) and M cells, which affects the coordination between photosynthetic and transpiration processes.

In *Oryza* species, there is a close negative relationship between leaf *A* and $C_i - C_c$ and a strong positive

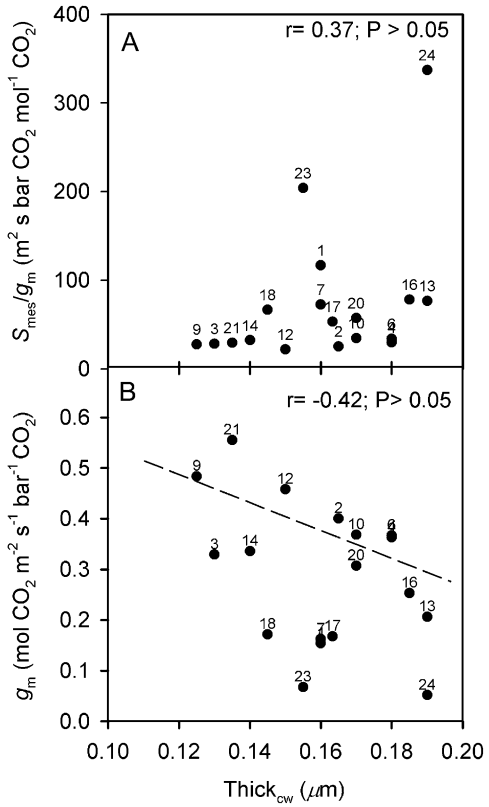

Figure 10. Correlations between $Thick_{cw}$ and functional traits in *Oryza* accessions. A, S_{mes}/g_m. B, g_m. Accessions above the dashed line have $g_m > 0.35$ mol CO_2 m^{-2} s^{-1} bar^{-1} CO_2 and show a negative relationship between g_m and g_{s_CO2} (Fig. 5C). Points are mean values per accession (SE values are given in Supplemental Table S3). Numbers correspond to the accessions listed in Table I.

correlation between A and C_c. A positive correlation between S_{mes} (or S_{chl}) and A, which was not found in this study, would have kept $C_i - C_c$ independent of A (Evans, 1999). In addition, a tendency for a negative correlation between $C_a - C_i$ and $C_i - C_c$ was observed ($P > 0.05$), and based on Equation 1, g_m together with g_s should be involved in the tradeoff between $C_a - C_i$ and $C_i - C_c$. In fact, there was a significant negative correlation between g_m and $C_i - C_c$ ($P < 0.01$); also, a tight positive association between S_{mes}/g_m and $C_i - C_c$ was found ($P < 0.01$). In this regard, Niinemets et al. (2009) described how a drawdown of CO_2 partial pressure from substomatal cavities to chloroplasts ($C_i - C_c$), rather than g_m per se, characterizes the M diffusion limitation of photosynthesis.

Across *Oryza* accessions the data suggest that a negative correlation exists between g_m and C_i ($P > 0.05$); a higher g_m when C_i is low could prevent C_c from becoming too low with loss of efficiency of Rubisco activity, while a lower g_m associated with a higher C_i tends to avoid excess C_c compared with Rubisco capacity. There is evidence for a strong inverse relationship between g_m and C_i when photosynthesis is not limited by CO_2 but by regeneration of Rubisco or triose phosphate utilization (Flexas et al., 2007). In addition, there is a weak negative association between g_s and $C_a - C_i$ and a strong negative correlation between g_s and $C_i - C_c$ ($P < 0.01$), which is partially driven by *O. brachyantha* and *O. coarctata* (data not shown). This is plausible, since $C_i - C_c$ is affected by the coordination between carboxylation activity and g_m, which can adjust faster than g_s, so that changes in $C_i - C_c$ may occur quicker than in $C_a - C_i$ (Flexas et al., 2007).

Relationships between Leaf Structural Traits and *A/E*

The results are consistent with the hypothesis that leaf structural traits in *Oryza* accessions are involved in the relationship between A and E, which affects A/E. Based on PFA, A/E was among the interrelated leaf traits (besides $Thick_{leaf}$ and a number of structural factors) that were positively associated with M architecture; vice versa, E showed a negative association. Trait-to-trait analysis also suggested a negative relationship between $Thick_{leaf}$ and E ($P > 0.05$), which reflects the negative correlation found between $Thick_{leaf}$ and g_s ($P > 0.05$). When excluding two outlier accessions (*O. brachyantha* 23 and *O. australiensis* 20), a significant negative association between $Thick_{leaf}$ and E was observed ($P < 0.01$; data not shown).

When considering features associated with photosynthesis, there was a close negative correlation ($P < 0.01$) between $Thick_{leaf}$ and C_i, which was mirrored by a corresponding positive correlation between $Thick_{leaf}$ and $C_a - C_i$. This suggests that C_c could potentially become more limiting for photosynthesis in thick leaves. With respect to leaf thickness, Parkhurst et al. (1988) reported that, in general, the activity of Rubisco varies through the M in response to a light gradient, making it possible to have a balance between local CO_2 pressures and local enzyme activities in a way that may increase the overall assimilation rate of the leaf. However, in the *Oryza* accessions $Thick_{leaf}$ was not positively associated with A. This result, which is in agreement with Niinemets (1999), can be explained by the lack of correlation between $Thick_{leaf}$ and g_m discussed earlier, by the tight negative relationship between $Thick_{leaf}$ and C_i (and a weak negative correlation between $Thick_{leaf}$ and g_s), and by the weak negative correlation between $Thick_{leaf}$ and $C_i - C_c$. In contrast, there is a significant positive correlation between $Thick_{leaf}$ and A_{max}; this may occur considering that saturating CO_2 will increase C_i and the $C_i - C_c$ gradient, promoting CO_2 diffusion to the chloroplasts.

With respect to stomata, there were positive associations between the stomatal density on the abaxial side of the lamina and features of both CO_2 and water exchange, but not on the adaxial side. The results suggest that the stomata on the abaxial side of the lamina are mainly conducting CO_2 and water vapor between the leaf and atmosphere; that is, the amphistomatous leaves of genus *Oryza* could functionally behave as hypostomatous, by closing or nearly closing the adaxial stomata (Reich, 1984). While a strong stomatal regulation on the adaxial side of leaves to limit water loss tends to occur naturally in leaves (Smith et al., 1997), it may have been intensified in this study by light exposure of the lamina in the cuvette.

The tendency for a negative correlation ($P > 0.05$) between $Thick_{leaf}$ and $D_{st}ab$, and a significant positive linkage between $D_{st}ab$ and both g_s and E, may explain the tendency for a negative association observed across *Oryza* accessions between $Thick_{leaf}$ and E. In addition, the leaf hydraulic architecture might contribute to the relationships between leaf structure and transpiration (Brodribb et al., 2007, 2010; Guyot et al., 2012). In this regard, bundle sheath extensions are known to facilitate leaf water conductivity through the M to the stomata (Sack and Holbrook, 2006). However, *O. coarctata* and *O. brachyantha*, which have prominent bundle sheath extensions toward the adaxial surface, have the majority of stomata located deep in the furrows between bundle sheaths. This leaf stomatal arrangement may provide an additional boundary layer resistance that limits E while maintaining a high leaf water potential. The structural design of *O. coarctata* appears to restrict the loss of water at the expense of photosynthesis (low A), by having the lowest g_s and g_m values and a low g_m/g_{s_CO2} ratio, with a high A/E (among the highest A/E and the highest A/g_{s_H2O} across *Oryza* accessions).

In summary, across *Oryza* accessions under current ambient CO_2 partial pressures and at 30°C leaf temperature, there is a positive significant association between $Thick_{leaf}$ and leaf A/E (this occurs with $Thick_{leaf}$ having a negative correlation with E and without a correlation with A across accessions). Higher levels of CO_2 can increase plant A/E by enhancing photosynthesis and decreasing water loss (due to a decrease in g_s with increasing CO_2; Long et al., 2004; Lammertsma

et al., 2011). In *Oryza* accessions under CO_2 saturating conditions, there is a positive correlation of A_{max} with $Thick_{leaf}$; thus, accessions having thicker leaves could especially benefit from increased photosynthesis and A/E above ambient levels of CO_2 (i.e. when CO_2 is not limiting).

Correlation between g_m/g_s Ratio and Leaf A/E

A high g_m/g_s ratio is considered favorable for increasing A/E (Flexas et al., 2008, 2013; Barbour et al., 2010). The hypothesis that the g_m/g_s ratio would positively correlate with leaf A/E in *Oryza* species was supported. Several accessions with g_m/g_{s_CO2} greater than 1.0 and high g_m values had medium to high A and A/g_{s_H2O} (and A/E) ratios. They were *O. australiensis* 21 and 22, *O. glaberrima* 2, *O. longistaminata* 4, *O. rufipogon* 9, *O. punctata* 12, and *O. latifolia* 19; in addition, they had relatively low S_{mes}/g_m. These accessions have leaf features that may be of value for maintaining carbon gain while conserving water. *O. rufipogon* (Zhao et al., 2008, 2010) and *O. australiensis* (Zhao et al., 2010) are two of the wild relative resources for crop improvement of *O. sativa*, and there is interest in *O. australiensis* and *O. glaberrima* for attributes associated with drought tolerance (see introduction).

The $\delta^{13}C$ has been used as an indicator of leaf A/E in several species (Flexas et al., 2008; Barbour et al., 2010), including rice (Dingkuhn et al., 1991; Kondo et al., 2004; Centritto et al., 2009; Xu et al., 2009). In this study on *Oryza* accessions a weak positive association between $\delta^{13}C$ and A/g_{s_H2O} was observed ($P > 0.05$). Interestingly, *O. glaberrima* 2 and *O. australiensis* 21 were outliers, having high A/g_{s_H2O} but among the most negative $\delta^{13}C$ values. In these two accessions, the high g_m with medium to high g_{s_H2O} values could maintain high C_c, A, and A/g_{s_H2O} with lower $\delta^{13}C$ values.

Leaf Traits Contributing to Plant Drought Tolerance

Plants have diverse leaf morphoanatomical and architectural adaptations to face the challenge of coordinating structural requirements for strength and durability, controlling rates of water loss, and functioning photosynthetically (light capture, facilitating the diffusion of CO_2 to the chloroplasts, and the development of metabolic capacity for carbon assimilation; Evans, 1999; Evans et al., 2004; Brodribb et al., 2010; Waite and Sack, 2010).

In this study, there was support for the hypothesis that a high g_m/g_s ratio is coordinated with M leaf traits to confer plant drought tolerance. In particular, the results indicate that a high g_m and g_m/g_s ratio, a low S_{mes}/g_m, along with a high M $Thick_{cw}$ are features that could be beneficial in warm climates and limited water availability. *O. glaberrima*, *O. meridionalis*, and *O. australiensis* 20, which are recognized as species having tolerance to drought, have relatively high $Thick_{cw}$ (greater than 0.165 μm) compared with most *Oryza* species. In addition, they have relatively high g_m and g_m/g_s ratio and low S_{mes}/g_m ratio despite having high $Thick_{cw}$; also, *O. longistaminata* 4 has similar features. Further study of these species is needed to determine the contribution of nonstructural factors to the relationships between high g_m, low S_{mes}/g_m ratio, and high cell wall thickness.

CONCLUSION

This study provides insight into the diversity of leaf structure and how it relates to photosynthesis and transpiration between representatives of cultivated rice (*O. sativa* and *O. glaberrima*) and a number of wild relatives in the genus *Oryza*. There are significant correlations between certain structural traits, between certain functional traits associated with photosynthesis and transpiration, and fewer correlations of function with individual structural traits. There is a close positive relationship between A and g_m, but neither of these two fundamental leaf functional traits is significantly correlated, at ambient CO_2 levels, with $Thick_{leaf}$ or any other single M structural feature. It is recognized that the value of g_m in plants depends on multiple structural traits that can covary between species with Thick leaf (which may include leaf S_{mes} and M cell features such as $Thick_{cw}$, cell volume, and Lob_{cell}); in addition, g_m may be affected by cell wall composition, along with biochemical factors controlling the levels and transport of inorganic carbon in the liquid phase from IAS to chloroplast stroma. Large differences were observed in leaf A/E, which is suggested to be dependent on a tradeoff between g_m and g_s, and leaf structural features (e.g. a positive correlation with leaf thickness). Interestingly, species were identified having high A/E while sustaining photosynthesis. They have high g_m values, along with high g_m/g_s ratios, low S_{mes}/g_m, and, in some species, relatively thick M cell walls, which could be beneficial traits for rice cultivated in warm climates and limiting availability of water.

MATERIALS AND METHODS

Plant Material

Accessions of *Oryza* species (listed in Table I) were grown in 3-L free-drainage pots in a controlled-environment growth chamber. The photoperiod was 12 h (8 AM to 8 PM standard time) with air temperature of 28°C, and the dark period was with air temperature of 25°C. Light was emitted by 400-W metal halide and high-pressure sodium lamps and supplied to the canopy in a bell-shaped pattern (by incremental changes in photosynthetically active photon flux density [PPFD] every 2 h) with maximum PPFD of 1,100 μmol photons m^{-2} s^{-1} for 4 h. Air relative humidity was kept at approximately 70%, which corresponded to a maximum air vapor pressure deficit of approximately 1.8 kPa.

Three plants per accession were grown (one per pot) in a Sunshine Mix LC-1 soil (Sun Gro Horticulture) mixed with turface (ratio of 3:1 in volume). They were irrigated daily and fertilized twice per week to pot saturation with a nutrient solution including Sprint 330 iron chelate (1.3 g L^{-1}), magnesium sulfate (0.6 g L^{-1}), Scotts-Peters Professional 10-30-20 compound (2.8 g L^{-1}), and Scott-Peters Soluble Trace Element Mix (8.0 mg L^{-1}; Scotts).

Throughout, *O. sativa* accessions are written in full. For the wild relatives, when multiple accessions were analyzed per species, the species name is

followed by the accession number (from Table I). Some figures identify accessions by the numbers in Table I (1–24); when referring to these figures, the accession number is always given.

Leaf and M Cell Structural Traits

Sample Preparation for Light and Electron Microscopy

The study of leaf anatomy was carried out on three 20- to 40-d-old plants per each *Oryza* accession marked with an asterisk in Table I (note that for *O. sativa* cv IR72 and *O. australiensis* 22, structural measurements were only made on stomata). On each plant, the midportion of fully expanded leaves (usually the third and fourth leaves from the apex on the central stem) was sampled. They were fixed at 4°C in 2% (v/v) paraformaldehyde and 2% (v/v) glutaraldehyde in 0.1 M phosphate buffer (pH 7.2), postfixed in 2% (w/v) OsO_4, and, after a standard acetone dehydration procedure, embedded in Spurr's epoxy resin. Leaf cross sections were made using a Reichert Ultracut R ultramicrotome (Reichert-Jung). For light microscopy, semithin leaf sections were stained with 1% (w/v) toluidine blue O in 1% (w/v) $Na_2B_4O_7$ and observed at 100× magnification with the Olympus BH-2 light microscope (Olympus Optical) equipped with LM Digital Camera & Software (Jenoptik ProgRes Camera, C12plus). For transmission electron microscopy, ultrathin leaf cross sections were stained with 4% (w/v) uranyl acetate followed by 2% (w/v) lead citrate. Transmission electron microscopes, H-600 (Hitachi) and JEM-1200 EX (JEOL USA) equipped with a MegaView III Digital Camera, and Soft Imaging System software were used for observation and photography.

Analyses of Leaf Cross Sections

Leaf and cell structural traits, which were determined from light and electron microscopy on leaf cross sections, are listed in Table II. For each accession, the micrographs analyzed were on two to three leaves, depending on the technical difficulty, with each leaf taken from a different plant (n = 2 or n = 3). All measurements were performed on digital images using an image-analysis program (UTHSCSA Image Tool for Windows, version 3.00; University of Texas Health Science Center). For a consistent protocol, measurements on leaf M cells from light and electron microscopy were made on the first cell layer facing the adaxial side of leaves. The appearance of the size and structure of M cells throughout a leaf cross section was similar except for the few distinctive paraveinal M cells (which are very large in some species), which were excluded from analysis.

Light Microscopy

From light microscopy images of leaf cross sections, $Thick_{leaf}$ (μm) was measured between the bundles and bulliform cells (Fig. 1A). The lumen a_{cell} (μm^2) was determined (and taken as a surrogate for M cell volume; see Supplemental Materials and Methods S1). From micrographs made on each leaf, 15 to 25 $Thick_{leaf}$ and a_{cell} measurements were taken, and the corresponding mean values per leaf were calculated.

The leaf M porosity (%), defined as Vol_{IAS}, was calculated as

$$Vol_{IAS} = \frac{a_{IAS}}{a_{tot\_M}} \quad (2)$$

where a_{tot_M} (μm^2) is the total area between epidermal layers (including M, air space, and vascular tissue) from measurement of the leaf cross sections and a_{IAS} (μm^2) is the area of the IAS in the leaf cross-section (Supplemental Fig. S2A).

The total length of M cell wall exposed to IAS (μm) and the width of the leaf cross section analyzed (μm) were measured, and the corresponding total S_{mes} ($\mu m^2\ \mu m^{-2}$) was inferred based on Evans et al. (1994) as:

$$S_{mes} = \frac{\text{Total length of M cell wall exposed to IAS}}{Section\_width} * F \quad (3)$$

where F is the curvature correction factor. A general prolate spheroid shape with the major axis being twice the length of the other two minor axes was assumed, as in Sage and Sage (2009) and Scafaro et al. (2011), and accordingly, based on Thain (1983), an F value of 1.42 was used.

Electron Microscopy

From electron micrographs of leaf cross sections, the total M cell wall length exposed to IAS covered by chloroplasts (μm) was determined; this was used as the numerator in Equation 3 (above) to calculate S_{chl} ($\mu m^2\ \mu m^{-2}$). The extent of Lob_{cell} was assumed to correspond to the cell perimeter tortuosity ($\mu m\ \mu m^{-1}$), which was determined from measurements on individual M cells (Supplemental Fig. S2B). In the absence of lobes, cell perimeter tortuosity = 1.0. Other structural measurements on M cells included $Thick_{cw}$ (μm), L_{cw_IAS} (μm), CW_{IAS} (%), length of a single cell wall exposed to intercellular air space covered by chloroplasts ($L_{cw\_IAS\_chl}$; μm), CW_{IAS_chl} (%), L_{ACW} (μm), L_{ACW_chl} (μm), ACW_{chl} (%), CW_{chl} (%), Vol_{chl} (%), Vol_{vac} (%), and minor diameters of mitochondria (μm). A minimum of 25 measurements per each M cell trait were taken on each leaf, and a mean value (per leaf) was calculated.

In addition, the mean P/a_{cell} ($\mu m\ \mu m^{-2}$) for each leaf analyzed was calculated, where P is the perimeter of the M cell section. P/a_{cell} was taken as a relative gauge of the ratio of M cell surface area/cell volume (Supplemental Materials and Methods S1).

Analysis of Leaf Surfaces

Images of the adaxial and abaxial epidermal surfaces were captured on three live leaves (each from different plants; n = 3) per *Oryza* accession under the low-vacuum mode with a Quanta 200F scanning electron microscope (FEI). For each leaf, stomatal pore length in the adaxial and abaxial lamina surface (L_{st}ad and L_{st}ab; μm) were calculated based on 10 to 25 measurements. The stomatal density on each leaf side was determined as D_{st}ad and D_{st}ab (mm^{-2}). For each leaf, stomatal pore area index (I_{st}, $mm^2\ mm^{-2}$) was calculated as an index of maximum stomatal pore area per lamina area based on Sack et al. (2003) as

$$I_{st} = D_{st} * L_{st}^2 \quad (4)$$

where D_{st} is the cumulative (adaxial plus abaxial) number of stomata per unit (one side) of lamina surface area and L_{st} is the mean stomatal pore length. In addition, the I_{st}ad and I_{st}ab were calculated.

Leaf Functional Measurements

Gas-Exchange Measurements: Equipment Setup and Protocol

Leaf-atmosphere CO_2 and H_2O exchange measurements were performed in Pullman, WA (mean atmospheric pressure of 92.1 kPa) using a LI-6400XT portable photosynthesis system equipped with a 6400-40 Leaf Chamber Fluorometer (LI-COR Biosciences). The Leaf Chamber Fluorometer is designed with a uniform, integrated red/blue light-emitted diode light source and a pulse-amplitude modulated (PAM) fluorometer enabling simultaneous measurement of chlorophyll fluorescence and gas exchange over the same leaf area of 2.0 cm^2. The fraction of blue light was set to 10% of the PPFD (μmol photons $m^{-2}\ s^{-1}$) to maximize stomatal aperture. A CO_2 cartridge was used, and a 6400-01 CO_2 Injector System controlled the CO_2 partial pressure entering the cuvette (C_a, μbar). The oxygen partial pressure entering the leaf cuvette was set by mixing different partial pressures of nitrogen and oxygen in a CO_2-free air stream through two mass flow controllers (MKS Instruments).

For all accessions of *Oryza* species in Table II, measurements were made on one leaf on three different plants (n = 3). In general, the same leaves, or leaves in the same position as those sampled for leaf anatomical survey, were chosen. The mid to distal portion of each leaf blade was inserted in the leaf chamber for gas-exchange measurements. For almost all *Oryza* accessions (except for *O. alta*, *O. latifolia* 18, and *O. longistaminata* 5), two leaf blades were used to cover the cuvette luminal surface area.

The data were acquired between 9 AM and 4 PM standard time in a room with air temperature around 30°C. Measurements were made after plants were acclimated for approximately 1 h. Leaf functional traits that were provided by leaf gas exchange are listed in Table II.

Leaf A-C_i Curves

A (μmol $CO_2\ m^{-2}\ s^{-1}$) and C_i (μbar) were determined at 184.2 mbar ambient oxygen partial pressure (near current ambient levels at the study site, and corresponding to 200 mmol oxygen mol^{-1} air). PPFD was set at 1,500 μmol photons $m^{-2}\ s^{-1}$, leaf temperature at 30°C, while leaf-to-air vapor pressure deficit was maintained between 1.0 and 1.5 kPa.

For each *Oryza* accession, an A-C_i response curve was acquired on three different plants at (decreasing) C_a from 350 to 18 μbar. In one of the replications, following measurements with decreasing CO_2, C_a was increased from 350 to 1,380 μbar to determine the A_{max} (μmol $CO_2\ m^{-2}\ s^{-1}$).

Kneading synthetic rubber (Terostat IX; Henkel Technologies) was put around the gaskets of the Leaf Chamber Fluorometer; this was to limit CO_2 diffusion leaks into and from the chamber when imposing C_a in the cuvette lumen below and above the CO_2 partial pressure in the outside air. In addition, the magnitude of the cuvette CO_2 diffusion leaks was estimated, and a CO_2 diffusion correction term was included in A and C_i computations (Supplemental Material and Methods S2).

For each A-C_i response curve, least-square regression analysis was applied to the initial slope ($C_i \leq 100$ μbar) to determine the CE (mol CO_2 m^{-2} s^{-1} bar^{-1} CO_2) and the Γ (μbar). Additionally, A, C_i, $C_a - C_i$, E (mmol water m^{-2} s^{-1}), and g_{s_H2O} (mol water m^{-2} s^{-1}) at 350 μbar C_a (near current ambient levels at the study site) were extracted from the data set, and the corresponding leaf A/E (μmol CO_2 $mmol^{-1}$ water) and A/g_{s_H2O} (μmol CO_2 mol^{-1} water) were calculated.

Also, g_{s_CO2} (mol CO_2 m^{-2} s^{-1}) was determined from g_{s_H20} as

$$g_{s\_CO_2} = \frac{g_{s\_H_2O}}{1.6} \quad (5)$$

where 1.6 is the ratio between the molecular diffusivities of water and CO_2 in air (Massman, 1998).

The data set submitted to statistical analysis was composed of three repetitions of A, CE, Γ, C_i, $C_a - C_i$, E, g_{s_H2O}, A/g_{s_H2O}, and A/E ($n = 3$) and one value of A_{max} ($n = 1$) for each *Oryza* accession.

Leaf Chlorophyll Fluorescence Measurements

Leaf chlorophyll fluorescence was measured using the 6400-40 fluorometer (LI-COR Biosciences) simultaneously while acquiring the A-Ci response curves. Steady-state fluorescence (F_s) and maximum fluorescence (F_m') were recorded after equilibration to a steady state. Maximum fluorescence was measured using a 0.8-s saturating pulse of light (approximately 8,000 μmol photons m^{-2} s^{-1} supplied by light-emitting diodes with peak emission at 630 nm).

Estimation of M Conductance to CO_2 Diffusion Based on Leaf Gas-Exchange and Chlorophyll Fluorescence Measurements

The combined leaf gas-exchange and chlorophyll fluorescence data from the A-C_i response curves were used to calculate g_m (mol CO_2 m^{-2} s^{-1} bar^{-1} CO_2) using the variable J method (Di Marco et al., 1990; Harley et al., 1992), applied as in Li et al. (2009). According to Genty et al. (1989), the total electron transport rate (J_T; μmol e^- m^{-2} s^{-1}) was determined as

$$J_T = \alpha_{leaf} * \beta * PPFD * \phi_{PSII} \quad (6)$$

where α_{leaf} is the leaf absorbance of photosynthetic quanta, β is the fraction of photons absorbed by PSII, PPFD (μmol photons m^{-2} s^{-1}) is the PPFD incident on the leaf, and ϕ_{PSII} is the photochemical yield of PSII. The default value taken for α_{leaf} was 0.85 (Li et al., 2009) and that for β was 0.45, assuming that approximately 45% of the photons are absorbed by PSII (Laisk et al., 2006). ϕ_{PSII} was computed as

$$\phi_{PSII} = \frac{(F_m' - F_s)}{F_m'} \quad (7)$$

Electron transport rates associated with carboxylation (J_c) and oxygenation (J_o) were calculated according to Epron et al. (1995) as

$$J_c = \frac{1}{3}[J_T + 8(A + R_d)] \quad (8)$$

and

$$J_o = \frac{2}{3}[J_T - 4(A + R_d)] \quad (9)$$

where A (μmol CO_2 m^{-2} s^{-1}) is the net photosynthetic rate per unit of leaf surface area and R_d (μmol CO_2 m^{-2} s^{-1}) is the corresponding mitochondrial respiration rate in the light (assumed to be 0.7 μmol CO_2 m^{-2} s^{-1} based on experimental measurements; data not shown). The C_c (μbar) was calculated according to Epron et al. (1995) as

$$C_c = C_i \frac{S_{in\_vivo\_VJ}}{S_{in\_vivo\_\Gamma^*}} \quad (10)$$

where $S_{in\_vivo\_VJ}$ is the in vivo apparent CO_2/oxygen specificity factor for Rubisco determined from the initial slope of the linear regression forced to the origin from plots of J_c/J_o versus C_i/oxygen partial pressure (at decreasing C_a from 350 μbar) and $S_{in\_vivo\_\Gamma^*}$ is the in vivo apparent CO_2/oxygen specificity factor for Rubisco associated with the photorespiratory compensation point (Γ^*; μbar) estimated by gas-exchange measurements. In this study, Γ^* was determined based on the method of Laisk (1977) at 184 mbar oxygen partial pressure and at 30°C leaf temperature. Four *Oryza* species were considered, two of them having among the lowest (*O. sativa* cv IR64 and *O. rufipogon* 8) and two among the highest (*O. glumaepatula* and *O. minuta*) Γ values; Γ^* ranged from 42 to 48 μbar.

The equation developed by Laing et al. (1974) and Jordan and Ogren (1984) describes the relationship between S and Γ^* as

$$\Gamma^* = \frac{k^* pO_2}{S} \quad (11)$$

where pO_2 (μbar) is air partial pressure of oxygen, k is the stoichiometry factor between carboxylase and oxygenase activity at the photorespiratory CO_2 compensation point, and S is the effective CO_2/oxygen specificity factor for Rubisco based on kinetic properties determined in vitro (bar bar^{-1}). $k = 0.5$ at the photorespiratory compensation point under the assumption that one CO_2 is generated in the glycolate pathway for every two oxygens reacting with ribulose-1,5-biphosphate.

The equation can be used to calculate the apparent Rubisco specificity factor $S_{in\_vivo\_\Gamma^*}$ from the measurement of Γ^* as

$$S_{in\_vivo\_\Gamma^*} = \frac{k^* pO_2}{\Gamma^*} \quad (12)$$

g_m (mol CO_2 m^{-2} s^{-1} bar^{-1} CO_2) was then calculated, based on Equation 1, as

$$g_m = \frac{A}{C_i - C_c} \quad (13)$$

where A, C_i, and C_c are as already defined. Per each leaf, the g_m values at C_a = 350 μbar were used in data analysis.

The ratio between g_m at C_a= 350 μbar and the corresponding g_{s_CO2} (g_m/g_{s_CO2}, bar^{-1} CO_2), and the ratio between S_{mes} and g_m (S_{mes}/g_m, m^2 s bar CO_2 mol^{-1} CO_2, which represents the M resistance to CO_2 diffusion per unit S_{mes} and is listed in Table II among the functional traits) were calculated. In particular, the terms included in g_m and the physical meaning of S_{mes}/g_m, based on Fick's laws, are described in Supplemental Materials and Methods S3.

Based on the protocol followed, three replications ($n = 3$) of C_c, $C_i - C_c$, g_m, g_m/g_{s_CO2}, and S_{mes}/g_m for each *Oryza* accession were used in the statistical analysis.

For comparison with the chlorophyll fluorescence method, M conductance was estimated on a few *Oryza* accessions based on simultaneous measurements of leaf gas exchange and ^{13}C isotope discrimination (Evans et al., 1986; Pons et al., 2009). Leaves of *O. sativa* cv IR64, *O. glaberrima* 2, *O. glumaepatula* 3, and *O. rufipogon* 9 were sampled according to the methodology described for leaf gas-exchange measurements. A LI-6400XT portable photosynthesis system equipped with a 6400-22L lighted opaque conifer chamber (LI-COR Biosciences) was used under the same environmental conditions described above for gas exchange measurements, except the C_a was 350 μbar. The LI-6400XT was coupled to a tunable-diode laser absorption spectroscope (TDLAS, model TGA 200A, Campbell Scientific) with a laser that measures CO_2 and ^{13}C (Bowling et al., 2003; Ubierna et al., 2013). M conductance calculations were performed based on the "single-point method" (Lloyd et al., 1992); they provided g_m values similar to those estimated by chlorophyll and gas-exchange measurements. Precisely, *O. sativa* cv IR64, *O. glaberrima* 2, *O. glumaepatula* 3, and *O. rufipogon* 9 showed mean g_m values of 0.342, 0.358, 0.411, and 0.457 mol CO_2 m^{-2} s^{-1} bar^{-1}, respectively (for comparison, see corresponding g_m data in Supplemental Table S3).

Stable Carbon Isotope Analysis of Leaf Biomass

A portion of each leaf used for the A-C_i response curve was collected for analysis of $\delta^{13}C$ (‰). Dried samples were combusted using a Eurovector elemental analyzer. The resulting nitrogen and CO_2 gases were separated by gas chromatography and admitted into the inlet of a Micromass Isoprime isotope ratio mass spectrometer for determination of $^{13}C/^{12}C$ ratio. $\delta^{13}C$ (‰) was used to represent the $^{13}C/^{12}C$ ratio of the leaf sample relative to the isotopic reference material Vienna Pee Dee Belemnite (Bender et al., 1973), and it was determined as

$$\delta^{13}C = \left[\left(\frac{R_{sample}}{R_{standard}}\right) - 1\right] * 1000 \quad (14)$$

where R_{sample} and $R_{standard}$ are the $^{13}C/^{12}C$ ratios of the leaf samples and the Vienna Pee Dee Belemnite limestone, respectively. Three repetitions of $\delta^{13}C$ ($n = 3$) were obtained for each *Oryza* accession.

Statistical Analyses

Statistical analyses were performed similar to Waite and Sack (2010) using SAS version 9.2 (SAS Institute). First, a three-stage (genomes, species, accessions) nested ANOVA was carried out to describe the variability of each structural and functional leaf trait, based on the entire data set for *Oryza* accessions. Significance for differences among genomes, species nested within genomes, and accessions nested within species and genomes was evaluated at $P < 0.05$, $0.01 \geq P \geq 0.001$, and $P < 0.001$.

PFA (Child, 2006) was run to identify the most important axes of covariation based on a total of 42 structural plus functional leaf traits (Table II). The mean values of each trait for each of 18 accessions were used. Based on a Varimax orthogonal rotation, eight factors associated with eigenvalues greater than 1 were retained. For each trait, factor loadings greater than 0.4 in absolute value were considered important; based on the size and the sign of the important loadings, a meaningful name was suggested for each of the first four PFA factors. The eight factor scores for each *Oryza* accession were computed. Since the PFA was conducted on a large set of leaf traits in relation to the number of accessions examined, this can reduce the power to detect the underlying factors (Osborne and Costello, 2004).

Pearson correlation matrices were calculated based on mean values of each leaf structural and functional trait per each *Oryza* accession to evaluate the trait-to-trait associations. The significance of correlation coefficients was determined at $P < 0.05$ and $P < 0.01$.

Supplemental Data

The following materials are available in the online version of this article.

Supplemental Figure S1. Scanning electron microscope images illustrating leaf surfaces of two *Oryza* species having different stomatal density and size.

Supplemental Figure S2. Example of a light microscopy image of a leaf cross section, and the scheme followed to estimate cell surface lobing.

Supplemental Table S1. Mean values, SE, and significance between *Oryza* genomes for each leaf structural and functional trait.

Supplemental Table S2. Mean values, SE, and significance between *Oryza* species (nested within genomes) for each leaf structural and functional trait.

Supplemental Table S3. Mean values, SE, and significance between *Oryza* accessions (nested within species and genomes) for each leaf structural and functional trait.

Supplemental Table S4. Leaf structural-functional PFA: factor loadings and factor scores on the first four main factors.

Supplemental Table S5. Pearson correlation matrix for leaf structural traits.

Supplemental Table S6. Pearson correlation matrix for leaf functional traits.

Supplemental Table S7. Portion of the Pearson correlation matrix for leaf structural to functional traits.

Supplemental Materials and Methods S1. Estimate of cell volume from values of a_{cell}.

Supplemental Materials and Methods S2. Magnitude of the CO_2 diffusion leaks into and from the Leaf Chamber Fluorometer and its effect on A and C_i calculations.

Supplemental Materials and Methods S3. Fick's laws applied to estimate g_m.

ACKNOWLEDGMENTS

We thank Berkley Walker for continuous advice and discussion on gas-exchange measurements, Dr. Ray W. Lee for performing the analysis of biomass carbon isotope composition, and Sandy Edwards for editing. We are grateful to the Franceschi Microscopy and Imaging Center at Washington State University for the use of its facilities and staff assistance and to Charles A. Cody for plant growth management.

Received March 5, 2013; accepted May 9, 2013; published May 13, 2013.

LITERATURE CITED

Aalto T, Juurola E (2002) A three-dimensional model of CO_2 transport in airspaces and mesophyll cells of a silver birch leaf. Plant Cell Environ **25:** 1399–1409

Barbour MM, Warren CR, Farquhar GD, Forrester GUY, Brown H (2010) Variability in mesophyll conductance between barley genotypes, and effects on transpiration efficiency and carbon isotope discrimination. Plant Cell Environ **33:** 1176–1185

Bender MM, Rouhani I, Vines HM, Black CC Jr (1973) $^{13}C/^{12}C$ ratio changes in Crassulacean acid metabolism plants. Plant Physiol **52:** 427–430

Bernacchi CJ, Portis AR, Nakano H, von Caemmerer S, Long SP (2002) Temperature response of mesophyll conductance: implications for the determination of Rubisco enzyme kinetics and for limitations to photosynthesis in vivo. Plant Physiol **130:** 1992–1998

Bowling DR, Sargent SD, Tanner BD, Ehleringer JR (2003) Tunable diode laser absorption spectroscopy for stable isotope studies of ecosystem-atmosphere CO_2 exchange. Agric Meteorol **118:** 1–19

Brar DS, Singh K (2011) *Oryza*. *In* C Kole, ed, Wild Crop Relatives: Genomics and Breeding Resources, Cereals. Springer-Verlag, Berlin, pp 321–365

Brodribb TJ, Field TS, Jordan GJ (2007) Leaf maximum photosynthetic rate and venation are linked by hydraulics. Plant Physiol **144:** 1890–1898

Brodribb TJ, Field TS, Sack L (2010) Viewing leaf structure and evolution from a hydraulic perspective. Funct Plant Biol **37:** 488–498

Burundukova OL, Zhuravlev Y-N, Solopov NV, Pyankov VI (2003) A method for calculating the volume and surface area in rice mesophyll cells. Russ J Plant Physiol **50:** 133–139

Busch FA, Sage TL, Cousins AB, Sage RF (2013) C_3 plants enhance rates of photosynthesis by reassimilating photorespired and respired CO_2. Plant Cell Environ **36:** 200–212

Centritto M, Lauteri M, Monteverdi MC, Serraj R (2009) Leaf gas exchange, carbon isotope discrimination, and grain yield in contrasting rice genotypes subjected to water deficits during the reproductive stage. J Exp Bot **60:** 2325–2339

Child D (2006) The Essentials of Factor Analysis, Ed 3. Continuum International Publishing Group, London

Di Marco G, Manes F, Tricoli D, Vitale E (1990) Fluorescence parameters measured concurrently with net photosynthesis to investigate chloroplastic CO_2 concentration in leaves of *Quercus ilex*. J Plant Physiol **136:** 538–543

Dingkuhn M, Farquhar GD, De Datta SK, O'Toole JC (1991) Discrimination of ^{13}C among upland rices having different water use efficiencies. Aust J Agric Res **42:** 1123–1131

Epron D, Godard D, Cornic G, Genty B (1995) Limitation of net CO_2 assimilation rate by internal resistances to CO_2 transfer in the leaves of two tree species (*Fagus sylvatica* L. and *Castanea sativa* Mill.). Plant Cell Environ **18:** 43–51

Evans JR (1999) Leaf anatomy enables more equal access to light and CO_2 between chloroplasts. New Phytol **143:** 93–104

Evans JR, Kaldenhoff R, Genty B, Terashima I (2009) Resistances along the CO_2 diffusion pathway inside leaves. J Exp Bot **60:** 2235–2248

Evans JR, Loreto F (2000) Acquisition and diffusion of CO_2 in higher plant leaves. *In* RC Leegood, TD Sharkey, S von Caemmerer, eds, Photosynthesis: Physiology and Metabolism. Kluwer Academic Publishers, Dordrecht, The Netherlands, pp 321–351

Evans JR, Sharkey TD, Berry JA, Farquhar GD (1986) Carbon isotope discrimination measured concurrently with gas exchange to investigate CO_2 diffusion in leaves of higher plants. Aust J Plant Physiol **13:** 281–292

Evans JR, Terashima I, Hanba Y, Loreto F (2004) CO_2 capture by the leaf. *In* WK Smith, TC Vogelmann, C Critchley, eds, Photosynthetic Adaptation: Chloroplast to the Landscape. Ecological Studies 178. Springer, New York, pp 107–132

Evans JR, von Caemmerer S (1996) Carbon dioxide diffusion inside leaves. Plant Physiol **110:** 339–346

Evans JR, von Caemmerer S, Setchell BA, Hudson GS (1994) The relationship between CO_2 transfer conductance and leaf anatomy in

transgenic tobacco with a reduced content of RuBiscCO. Funct Plant Biol **21:** 475–495

Farquhar GD, Ehleringer JR, Hubick KT (1989) Carbon isotope discrimination and photosynthesis. Annu Rev Plant Physiol Plant Mol Biol **40:** 503–537

Farquhar GD, Sharkey TD (1982) Stomatal conductance and photosynthesis. Annu Rev Plant Physiol **33:** 317–345

Flexas J, Bota J, Galmés J, Medrano H, Ribas-Carbó M (2006) Keeping a positive carbon balance under adverse conditions: responses of photosynthesis and respiration to water stress. Physiol Plant **127:** 343–352

Flexas J, Diaz-Espejo A, Galmés J, Kaldenhoff R, Medrano H, Ribas-Carbo M (2007) Rapid variations of mesophyll conductance in response to changes in CO_2 concentration around leaves. Plant Cell Environ **30:** 1284–1298

Flexas J, Niinemets U, Gallé A, Barbour MM, Centritto M, Diaz-Espejo A, Douthe C, Galmés J, Ribas-Carbo M, Rodriguez PL et al (2013) Diffusional conductances to CO_2 as a target for increasing photosynthesis and photosynthetic water-use efficiency. Photosynth Res (in press)

Flexas J, Ribas-Carbó M, Diaz-Espejo A, Galmés J, Medrano H (2008) Mesophyll conductance to CO_2: current knowledge and future prospects. Plant Cell Environ **31:** 602–621

Foster JR, Smith WK (1986) Influence of stomatal distribution on transpiration in low-wind environments. Plant Cell Environ **9:** 751–759

Genty B, Briantais J-M, Baker NR (1989) The relationship between the quantum yield of photosynthetic electron transport and quenching of chlorophyll fluorescence. Biochim Biophys Acta **990:** 87–92

Guyot G, Scoffoni C, Sack L (2012) Combined impacts of irradiance and dehydration on leaf hydraulic conductance: insights into vulnerability and stomatal control. Plant Cell Environ **35:** 857–871

Hanba YT, Miyazawa SI, Terashima I (1999) The influence of leaf thickness of the CO_2 transfer conductance and leaf stable carbon isotope ratio for some evergreen tree species in Japanese warm-temperature forests. Funct Ecol **13:** 632–639

Hanba YT, Shibasaka M, Hayashi Y, Hayakawa T, Kasamo K, Terashima I, Katsuhara M (2004) Overexpression of the barley aquaporin HvPIP2; 1 increases internal CO_2 conductance and CO_2 assimilation in the leaves of transgenic rice plants. Plant Cell Physiol **45:** 521–529

Harley PC, Loreto F, Di Marco G, Sharkey TD (1992) Theoretical considerations when estimating the mesophyll conductance to CO_2 flux by analysis of the response of photosynthesis to CO_2. Plant Physiol **98:** 1429–1436

Henry R, Rice N, Waters D, Kasem S, Ishikawa R, Hao Y, Dillon S, Crayn D, Wing R, Vaughan D (2010) Australian *Oryza*: utility and conservation. Rice **3:** 235–241

Jagadish KSV, Cairns JE, Kumar A, Somayanda IM, Craufurd PQ (2011) Does susceptibility to heat stress confound screening for drought tolerance in rice? Funct Plant Biol **38:** 261–269

Jarvis PG, Morison JIL (1981) The control of transpiration and photosynthesis by stomata. *In* PG Jarvis, TA Mansfield, eds, Stomatal Physiology. Cambridge University Press, Cambridge, UK, pp 247–279

Jordan DB, Ogren WL (1984) The CO_2/O_2 specificity of ribulose 1,5-bisphosphate carboxylase oxygenase-dependence on ribulose bisphosphate concentration, pH and temperature. Planta **161:** 308–313

Kellogg E (2009) The evolutionary history of Ehrhartoideae, Oryzeae, and *Oryza*. Rice **2:** 1–14

Kiirats O, Lea PJ, Franceschi VR, Edwards GE (2002) Bundle sheath diffusive resistance to CO_2 and effectiveness of C_4 photosynthesis and refixation of photorespired CO_2 in a C_4 cycle mutant and wild-type *Amaranthus edulis.* Plant Physiol **130:** 964–976

Kogami H, Hanba YT, Kibe T, Terashima I, Masuzawa T (2001) CO_2 transfer conductance, leaf structure and carbon isotope composition of *Polygonum cuspidatum* leaves from low and high altitudes. Plant Cell Environ **24:** 529–538

Kondo M, Pablico P, Aragones D, Agbisit R (2004) Genotypic variations in carbon isotope discrimination, transpiration efficiency, and biomass production in rice as affected by soil water conditions and N. Plant Soil **267:** 165–177

Laing WA, Ogren WL, Hageman RH (1974) Regulation of soybean net photosynthetic CO_2 fixation by the interaction of CO_2, O_2, and ribulose 1,5-diphosphate carboxylase. Plant Physiol **54:** 678–685

Laisk AK (1977) Kinetics of Photosynthesis and Photorespiration in C_3 Plants. Nauka, Moscow

Laisk AK, Eichelmann H, Oja V, Rasulov B, Rämma H (2006) Photosystem II cycle and alternative electron flow in leaves. Plant Cell Physiol **47:** 972–983

Lammertsma EI, de Boer HJ, Dekker SC, Dilcher DL, Lotter AF, Wagner-Cremer F (2011) Global CO_2 rise leads to reduced maximum stomatal conductance in Florida vegetation. Proc Natl Acad Sci USA **108:** 4035–4040

Li Y, Gao Y, Xu X, Shen Q, Guo S (2009) Light-saturated photosynthetic rate in high-nitrogen rice (*Oryza sativa* L.) leaves is related to chloroplastic CO_2 concentration. J Exp Bot **60:** 2351–2360

Lloyd J, Syvertsen JP, Kriedeman PE, Farquhar GD (1992) Low conductances for CO_2 diffusion from stomata to the sites of carboxylation in leaves of woody species. Plant Cell Environ **15:** 873–899

Long SP, Ainsworth EA, Rogers A, Ort DR (2004) Rising atmospheric carbon dioxide: plants FACE the future. Annu Rev Plant Biol **55:** 591–628

Massman WJ (1998) A review of the molecular diffusivities of H_2O, CO_2, CH_4, CO, O_3, SO_2, NH_3, N_2O, NO and NO_2 in air, O_2 and N_2 near STP. Atmos Environ **32:** 1111–1127

Ndjiondjop MN, Cisse F, Girma G, Sow M, Bocco M, Djedatin G, Blandine F (2010) Morpho-agronomic and molecular characterisation of *Oryza glaberrima* germplasm from Mali. Afr J Biotechnol **9:** 7409–7417

Niinemets Ü (1999) Components of leaf dry mass per area–thickness and density–alter leaf photosynthetic capacity in reverse directions in woody plants. New Phytol **144:** 35–47

Niinemets Ü, Díaz-Espejo A, Flexas J, Galmés J, Warren CR (2009) Role of mesophyll diffusion conductance in constraining potential photosynthetic productivity in the field. J Exp Bot **60:** 2249–2270

Nobel PS (2009) Physicochemical and Environmental Plant Physiology, Ed 4. Academic Press, San Diego

Nobel PS, Zaragoza LJ, Smith WK (1975) Relation between mesophyll surface area, photosynthetic rate, and illumination level during development for leaves of *Plectranthus parviflorus* Henckel. Plant Physiol **55:** 1067–1070

Ocheltree TW, Nippert JB, Prasad PV (2012) Changes in stomatal conductance along grass blades reflect changes in leaf structure. Plant Cell Environ **35:** 1040–1049

Oguchi R, Hikosaka K, Hirose T (2003) Does the photosynthetic light-acclimation need change in leaf anatomy? Plant Cell Environ **26:** 505–512

Osborne JW, Costello AB (2004) Sample size and subject to item ratio in principal components analysis. Pract Assess Res Eval **9:** http://pareonline.net/getvn.asp?v=9&n=11

Parker ML, Ford MA (1982) The structure of the mesophyll of flag leaves in three *Triticum* species. Ann Bot (Lond) **49:** 165–176

Parkhurst DF, Wong SC, Farquhar GD, Cowan IR (1988) Gradients of intercellular CO_2 levels across the leaf mesophyll. Plant Physiol **86:** 1032–1037

Peña-Rojas K, Aranda X, Joffre R, Fleck I (2005) Leaf morphology, photochemistry and water status changes in resprouting *Quercus ilex* during drought. Funct Plant Biol **32:** 117–130

Peterhansel C, Maurino VG (2011) Photorespiration redesigned. Plant Physiol **155:** 49–55

Pons TL, Flexas J, von Caemmerer S, Evans JR, Genty B, Ribas-Carbo M, Brugnoli E (2009) Estimating mesophyll conductance to CO_2: methodology, potential errors, and recommendations. J Exp Bot **60:** 2217–2234

Reich PB (1984) Leaf stomatal density and diffusive conductance in three amphistomatous hybrid poplar cultivars. New Phytol **98:** 231–239

Sack L, Cowan PD, Prasad PVV (2003) The 'hydrology' of leaves: coordination of structure and function in temperate woody species. Plant Cell Environ **26:** 1343–1356

Sack L, Holbrook NM (2006) Leaf hydraulics. Annu Rev Plant Biol **57:** 361–381

Sage TL, Sage RF (2009) The functional anatomy of rice leaves: implications for refixation of photorespiratory CO_2 and efforts to engineer C_4 photosynthesis into rice. Plant Cell Physiol **50:** 756–772

Scafaro AP, Von Caemmerer S, Evans JR, Atwell BJ (2011) Temperature response of mesophyll conductance in cultivated and wild *Oryza* species with contrasting mesophyll cell wall thickness. Plant Cell Environ **34:** 1999–2008

Scafaro AP, Yamori W, Carmo-Silva AE, Salvucci ME, von Caemmerer S, Atwell BJ (2012) Rubisco activity is associated with photosynthetic thermotolerance in a wild rice (*Oryza meridionalis*). Physiol Plant **146:** 99–109

Sengupta S, Majumder AL (2010) *Porteresia coarctata* (Roxb.) Tateoka, a wild rice: a potential model for studying salt-stress biology in rice. Plant Cell Environ **33:** 526–542

Slaton MR, Smith WK (2002) Mesophyll architecture and cell exposure to intercellular air apace in alpine, desert, and forest species. Int J Plant Sci **163:** 937–948

Smith WK, Vogelmann TC, DeLucia EH, Bell DT, Shepherd KA (1997) Leaf form and photosynthesis. Bioscience **47:** 785–793

Steppe K, Niinemets Ü, Teskey RO (2011) Tree size- and age-related changes in leaf physiology and their influence on carbon gain. *In* FC Meinzer, B Lachenbruch, TE Dawson, eds, Size- and Age-Related Changes in Tree Structure and Function. Springer, Dordrecht, The Netherlands, pp 235–253

Terashima I, Hanba YT, Tazoe Y, Vyas P, Yano S (2006) Irradiance and phenotype: comparative eco-development of sun and shade leaves in relation to photosynthetic CO_2 diffusion. J Exp Bot **57:** 343–354

Terashima I, Hanba YT, Tholen D, Niinemets Ü (2011) Leaf functional anatomy in relation to photosynthesis. Plant Physiol **155:** 108–116

Terashima I, Miyazawa SI, Hanba YT (2001) Why are sun leaves thicker than shade leaves? Consideration based on analyses of CO_2 diffusion in the leaf. J Plant Res **114:** 93–105

Terashima I, Ono K (2002) Effects of $HgCl_2$ on CO_2 dependence of leaf photosynthesis: evidence indicating involvement of aquaporins in CO_2 diffusion across the plasma membrane. Plant Cell Physiol **43:** 70–78

Terashima I, Saeki T (1983) Light environment within a leaf. I. Optical properties of paradermal sections of *Camellia* leaves with special reference to differences in the optical properties of palisade and spongy tissues. Plant Cell Physiol **24:** 1493–1501

Thain JF (1983) Curvature correction factors in the measurements of cell surface areas in plant tissues. J Exp Bot **34:** 87–94

Tholen D, Ethier G, Genty B, Pepin S, Zhu X-G (2012) Variable mesophyll conductance revisited: theoretical background and experimental implications. Plant Cell Environ **35:** 2087–2103

Tholen D, Zhu X-G (2011) The mechanistic basis of internal conductance: a theoretical analysis of mesophyll cell photosynthesis and CO_2 diffusion. Plant Physiol **156:** 90–105

Tosens T, Niinemets Ü, Vislap V, Eichelmann H, Castro Díez P (2012) Developmental changes in mesophyll diffusion conductance and photosynthetic capacity under different light and water availabilities in *Populus tremula*: how structure constrains function. Plant Cell Environ **35:** 839–856

Ubierna N, Sun W, Kramer DM, Cousins AB (2013) The efficiency of C_4 photosynthesis under low light conditions in *Zea mays*, *Miscanthus* × *giganteus* and *Flaveria bidentis*. Plant Cell Environ **36:** 365–381

Uehlein N, Otto B, Hanson DT, Fischer M, McDowell N, Kaldenhoff R (2008) Function of *Nicotiana tabacum* aquaporins as chloroplast gas pores challenges the concept of membrane CO_2 permeability. Plant Cell **20:** 648–657

Vaughan DA (1994) The Wild Relatives of Rice: A Genetic Handbook. International Rice Research Institute, Manila, The Philippines

Vaughan DA, Lu BR, Tomooka N (2008) The evolving story of rice evolution. Plant Sci **174:** 394–408

Vogelmann TC, Bornman JF, Josserand S (1989) Photosynthetic light gradients and spectral regime within leaves of *Medicago sativa*. Philos Trans R Soc Lond B **323:** 411–421

Waite M, Sack L (2010) How does moss photosynthesis relate to leaf and canopy structure? Trait relationships for 10 Hawaiian species of contrasting light habitats. New Phytol **185:** 156–172

Woolley JT (1983) Maintenance of air in intercellular spaces of plants. Plant Physiol **72:** 989–991

Xu Y, This D, Pausch RC, Vonhof WM, Coburn JR, Comstock JP, McCouch SR (2009) Leaf-level water use efficiency determined by carbon isotope discrimination in rice seedlings: genetic variation associated with population structure and QTL mapping. Theor Appl Genet **118:** 1065–1081

Zhao M, Acuña TLB, Lafitte HR, Dimayuga G, Sacks E (2008) Perennial hybrids of *Oryza sativa* × *Oryza rufipogon*. II. Carbon exchange and assimilate partitioning. Field Crops Res **106:** 214–223

Zhao M, Ding Z, Lafitte R, Sacks E, Dimayuga G, Holt D (2010) Photosynthetic characteristics in *Oryza* species. Photosynthetica **48:** 234–240